Climate Dynamics manuscript No.
(will be inserted by the editor)

The role of peninsular India in the South Asian summer monsoon

A. G. Turner · G. M. Martin · R. C. Levine

Received: date / Accepted: date

Abstract In this study we examine the role of the South Asian peninsula on the summer circulation and precipitation distribution in the Asian monsoon region using a series of novel atmosphere-only experiments with the Met Office Unified Model (MetUM) Global Atmosphere 3/Global Land 3 (GA3/GL3). Sensitivity to the topography, orography and land surface properties are examined separately. While the model usually features a strong dry bias centred on India as is common in CMIP3 and CMIP5 models, experiments replacing the Indian peninsula with a sea surface suggest a redistribution of precipitation in the northern Indian Ocean and enhanced precipitation in place of India. In further experiments, the role of land surface characteristics and orography (primarily the Western Ghats) of peninsular India are examined. The Western Ghats are shown to slow the flow across the peninsula and add a southerly component as the flow reaches the Bay of Bengal, as well as providing orographic enhancement resulting in upstream rainfall. Analysis of the evolution of turbulent surface fluxes and the boundary layer in wet-surface experiments shows a reduction in the diurnal cycle of sensible heating, enhancement of latent heating throughout the day, and increases in cumulus-capped boundary layers. More detailed lake experiments demonstrate a strong dependence of the strength of the diurnal cycle on lake heat capacity. So the presence of land at the surface restricts the availability of moisture but

A. G. Turner
NCAS-Climate,
Department of Meteorology, University of Reading,
Reading RG6 6BB, UK
Tel.: +44-118-3786019
Fax: +44-118-3788905
E-mail: a.g.turner@reading.ac.uk

G. M. Martin, R. C. Levine
Hadley Centre, Met Office,
FitzRoy Road,
Exeter, EX1 3PB, UK

amplifies the diurnal cycle. Finally, we perturb the Indo-Gangetic Plains region south of the Himalayas and demonstrate that the monsoon rainfall and circulation are very sensitive to changes in this region. In all the wet surface experiments in which mean rainfall is enhanced, deep convection becomes more preferable and there is evidence for more monsoon depressions and northward propagating intraseasonal variability.

Keywords Land-sea contrast · Monsoon · Model bias · Land-atmosphere interaction · South Asia

1 Introduction

The Asian summer monsoon supplies around 80% of annual rainfall to South Asia and affects the lives of more than a billion people who rely on it for agriculture and industry. Therefore being able to model and forecast the monsoon and make projections of future climate change are important goals for atmospheric science. While the models from the fifth Coupled Model Intercomparison Project (CMIP5) can produce a reasonable simulation of the gross features of the Asian monsoon, including its cross-equatorial flow, there are still large rainfall biases in most CMIP3 and CMIP5 models (Sperber *et al.*, 2012). Coupled GCMs can generally pick up some of the broad features of monsoon rainfall such as rainfall maxima just west of the Western Ghat mountains in India and in the Bay of Bengal, but the rainfall biases largely comprise too much rainfall over the Western Equatorial Indian Ocean (see also Bollasina and Nigam, 2009), and dry biases over India. As in Sperber *et al.* (2012) (Fig. 2), the dry biases over India are often over the north-east part of the peninsula, a region characterised by the monsoon trough and affected by low pressure systems, known as monsoon depressions when large (Krishnamurthy and Ajayamohan, 2010).

The origin of these biases over India is not understood, but cold biases in the simulation of winter and spring Arabian Sea sea-surface temperature (SST) are known to be detrimental to monsoon precipitation (Levine and Turner, 2012; Turner *et al.*, 2012; Levine *et al.*, 2013; Marathayil *et al.*, 2013). However dry biases exist in atmosphere-only integrations irrespective of coupling with the ocean, there are feedbacks between Indian and WEIO rainfall biases and there are known sensitivities to convective parameterisation (e.g. Bush *et al.*, 2013). The monsoon trough region and northern plains of India are also particularly interesting owing to the large population density and prevalence of irrigated agriculture in the Indo-Gangetic Plains. Despite the proximity to the Himalaya, most of the river flow in the Ganga comes from monsoon rainfall rather than glacial melt (Immerzeel *et al.*, 2010). Northern India was also identified by Koster *et al.* (2004) as one of only a few hotspots of land-atmosphere interaction, that is, a region of strong coupling between the land surface and atmosphere on seasonal time scales.

Ideas about the formation of the monsoon started centuries ago with Halley in 1686 (see the review in Turner and Annamalai, 2012). At the most basic level a meridional contrast in surface temperature caused by differential heat capacity leads to a surface pressure gradient and a meridional overturning circulation involving a cross-equatorial flow at the surface. This flow advects moisture to the South Asian subcontinent in the familiar southwesterly direction, aided by the planetary rotation. Li and Yanai (1996) further added the role of the Tibetan Plateau as a source of strong sensible heating in spring, leading to the meridional contrast in temperature extending to a significant depth of the troposphere, unlike other monsoon regions. More recently, Boos and Kuang (2010) have used GCM experiments to demonstrate that the narrow Himalayan range is fundamental to the monsoon, acting as a mechanical block to dry midlatitude westerlies interfering with the moist air originating over the Indian Ocean. Studies such as those of Chou *et al.* (2001) and Chou and Neelin (2003) have expanded on simple land-sea contrast ideas, pointing out that the net flux of energy into the atmospheric column is positive far north of the monsoon domain. The northward extent of the monsoon and location of the maximum ascent and rainfall can be further related to the position of the maximum sub-cloud moist static energy (Prive and Plumb, 2007), approximately coinciding with the Himalaya. For further discussion see the review in Turner and Annamalai (2012).

Although considerable work has been done on the effect of Himalaya/Tibetan Plateau uplift on the monsoon (Molnar *et al.*, 1993; Zhisheng *et al.*, 2001), we know less about the role of peninsular India itself in monsoon formation and maintenance. Bollasina and Nigam (2011b) have described the formation of the Pakistan heat low (at the western end of the monsoon trough that forms south of the Himalaya) prior to the monsoon, and shown that the Hindu Kush mountains are more important than local land surface heating in its development. Further deepening of the low during July is remotely forced by deep convection in the Bay of Bengal and eastern India, perhaps via a Rossby wave mechanism (e.g. Chou *et al.*, 2001). Bollasina and Nigam (2011a) have further described interactions between the Thar desert in north west India and heavy precipitation in the Bay of Bengal, by artificially expanding the desert. They confirm the regional large-scale feedback, finding enhanced precipitation to the east over Indochina when the desert is expanded.

In this study we aim to examine the role of the Indian subcontinent in the development of the South Asian monsoon in a GCM in a series of novel experiments in which we perturb the land surface and orography of the local region. We also examine the importance of the Indo-Gangetic Plains. We will use the Met Office global GCM MetUM GA3/GL3 and by analysing details of modelled boundary layer and convective behaviour hope also to learn something about monsoon precipitation biases in models.

In Section 2 we describe the methods used, while the seasonal mean results are shown in Section 3. In Section 4 we show changes to synoptic and intraseasonal variability, while discussion of the seasonal and diurnal evolution of surface fluxes and the boundary layer is made in Section 5. We conclude in Section 6.

2 Methods

In this section we describe the GCM used and the design of the experiments testing the role of peninsular India.

2.1 The MetUM GA3/GL3 model

The Met Office Unified Model (MetUM) is used with its Global Atmosphere 3/Global Land 3 configuration (GA3/GL3 Walters *et al.*, 2011), integrated at a resolution of 1.875° × 1.25° in longitude and latitude respectively (known as N96 resolution). There are 85 levels in the vertical, featuring a well resolved stratosphere. MetUM GA3/GL3 is currently classed as a development version of the Met Office Unified Model, meaning it undergoes regular updates in which new model physics are evaluated.

The model boundary layer scheme, included to parametrize turbulent motions, is as described in Lock *et al.* (2000) with modifications as in Lock (2001) and Brown *et al.* (2008). The scheme classifies seven types of boundary layer: stable; stratocumulus (Sc) over a stable layer; well mixed; decoupled stratocumulus with no cumulus present; decoupled stratocumulus lying over cumulus cloud; cumulus capped (Cu) and shear driven. The distribution of types is discussed later in Section 5.

The convection scheme is derived from Gregory and Rowntree (1990) but with major modifications, representing the average properties of an ensemble of convective plumes. Convection is triggered from the boundary layer using an undilute parcel, forming either shallow or deep convection. Mid-level convection can also be triggered from the free troposphere, when on top of a well-mixed or stable boundary layer. Precipitation from mid-level convection can be quite substantial if the appropriate boundary layer is low enough. For a detailed description of the convection scheme changes since the original version, see Bush *et al.* (2013).

The land surface scheme, JULES (Joint UK Land Environment Simulator, Best *et al.*, 2011; Clark *et al.*, 2011), represents a series of 9 land surface types at the sub-grid scale. These surface types are specified as a fractional fixed proportion of each N96 grid box, being one of: broadleaf trees; needleleaf trees; C3 crops/grasses; C4 crops/grasses; shrubs; urban; inland lake; bare soil; and land-ice. Proportions of the first eight classes in a grid box must sum to 1 or alternatively a grid square can be exclusively covered by land ice. The lake scheme, which we shall employ in some experiments, consists of a freely evaporating surface canopy combined with an effective heat capacity that represents a user-defined depth of water.

The dominant land surface types over India in MetUM GA3/GL3 are shown in Fig. 1, being mainly C3 grasses, with some broadleaf trees on the west coast and in east-central India where they make up to 40% of the surface. We do not show the percentage coverage of each class separately for brevity, but these regions also feature between 20% and 30% shrubs. Bare soil forms up to 20% of the land use across the country. In the Indo-Gangetic Plains region (particularly the foothills of the Himalaya) C3 grasses form up to 60% of the surface, reflecting the intensive agriculture there. The original land use classes in MetUM GA3/GL3 were compiled from an IGBP dataset (Global Soil Data Task, 2000). Analysis of a more recent NRSC/AwiFS characterisation of the Indian land surface at a higher resolution and featuring 24 classes (personal communication, A. Mitra of NCMRWF (India), February 2013), there is particular incidence of irrigated cropland in the northern plains. We remind the reader that the purpose of this study is not to present the results of more realistic land use settings for India, but to examine more fundamentally the role of the peninsula in the South Asian summer monsoon. We run the land surface model with fixed (i.e., non-dynamic) vegetation.

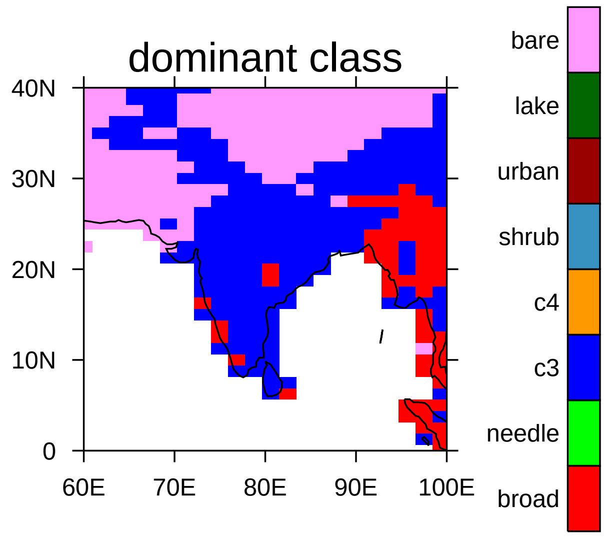

Fig. 1 Dominant class of land use proportions in each grid box of South Asia in MetUM GA3/GL3. Classes used are broadleaf trees; needleleaf trees; C3 crops/grasses; C4 crops/grasses; shrubs; urban; inland lake; and bare soil. Land-ice is excluded here.

In the vertical, the land surface scheme consists of four soil layers of thicknesses 10cm, 25cm, 65cm and 2m, totalling 3m.

The monsoon in MetUM GA3/GL3 GA3

Here we use the Global Precipitation Climatology Project (GPCP) monthly 2.5° data (Adler *et al.*, 2003), a merger of gauge readings and combined infrared/microwave satellite rainfall estimates to compare with the monsoon precipitation in MetUM GA3/GL3. Lower tropospheric winds at 850hPa are used to measure the mean monsoon flow, in comparison with those in the ERA-Interim Reanalysis (Dee *et al.*, 2011). Both data sets are curtailed to the 1983–2002 period to match the model integrations. In Figure 2 we show the simulation of the summer monsoon climate in MetUM

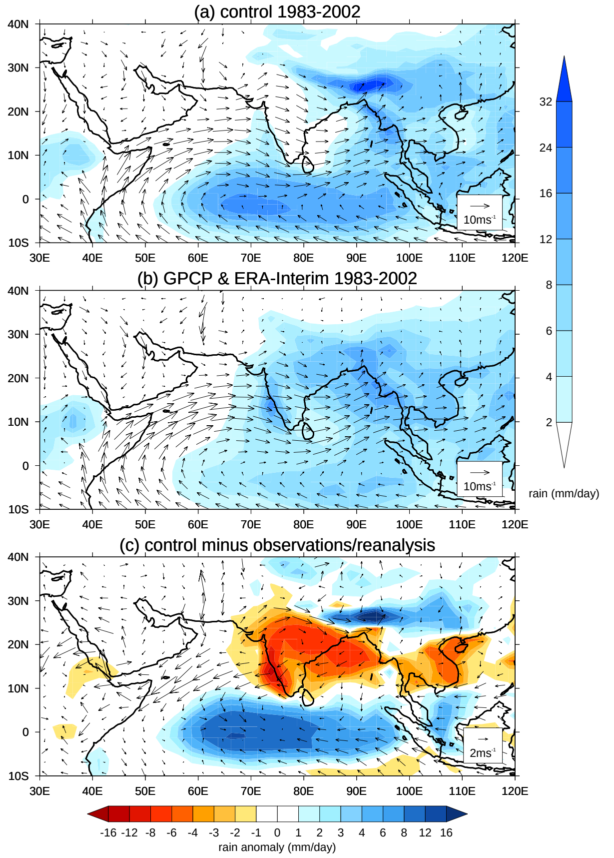

Fig. 2 Summer (JJAS) monsoon climate in the (a) MetUM GA3/GL3 *control* integration showing daily mean precipitation and lower tropospheric (850hPa) winds; (b) GPCP precipitation and ERA-Interim winds and (c) differences between MetUM GA3/GL3 precipitation and winds versus GPCP and ERA-Interim respectively. When calculating the differences, MetUM GA3/GL3 precipitation was downgraded to the 2.5° resolution of GPCP, while ERA-Interim winds were downgraded to the same grid as MetUM GA3/GL3. Units are mm day^{-1} and ms^{-1} respectively. Unit vectors are 10ms^{-1} and 2ms^{-1} for the climatologies and difference respectively.

GA3/GL3 in the *control* integration (see Section 2.2), averaged from 1983–2002, in comparison with GPCP and ERA-Interim observations for the same period.

The main features of the monsoon flow, including the large-scale cross equatorial flow associated with the Somali jet and its recurvature around the monsoon trough in northern India, are well captured. There is a slight tendency for the flow to diverge somewhat to the north and south as it reaches the west coast of India, as if it were attempting to go around the Western Ghats mountains on the coast. The main bias in the flow is a too weak Somali jet as it crosses the Arabian Sea, together with anomalous northwesterly flow along the Himalayan foothills (the north side of the monsoon trough), indicating a weakened trough.

The precipitation field demonstrates the rainfall maxima upstream of the Western Ghats, in the central/east Bay of Bengal upstream of the Arakan Range mountains in Burma, and also along the Himalayan foothills. The major biases in the model are dryness over the South Asian monsoon region, particularly in central India, a region often affected by monsoon depressions as they track westwards from the Bay of Bengal. There is also excessive rainfall in the western equatorial Indian Ocean (WEIO). Despite the large size of these rainfall biases, both are widespread in the CMIP3 and CMIP5 models (Sperber *et al.*, 2012) and indeed part of the motivation here is to explore the sensitivity of these biases to perturbations made to the South Asian peninsula. The largest wind biases mentioned above are consistent with reduced diabatic heating from the monsoon rainfall and are again prevalent in CMIP3 and CMIP5 models (Sperber *et al.*, 2012).

While the model used here is in atmosphere-only configuration, the errors shown in Fig. 2 are not due to the lack of coupling with the ocean. Levine and Turner (2012) have shown in a version of this model that introducing coupling with the ocean further limits South Asian monsoon precipitation, due to the development of cold biases in the Arabian Sea, which limit moisture advection. Such cold biases are also prevalent in the CMIP3 models (Marathayil *et al.*, 2013).

2.2 Experimental design

A series of experiments are performed using the MetUM GA3/GL3 model used in atmosphere-only configuration with AMIP (Atmospheric Model Intercomparison Project) SST forcing. All integrations are run from September 1981 to December 2002; the first 16 months are discarded as a cautious spin-up period to the altered initial conditions, leaving 20 years of output data for analysis (1983–2002). All experiments used are listed in Table 1 with the main ones being described below; more details are given later in the main text.

Figure 3 shows the original model land-sea mask at N96 resolution ($1.875^{\circ} \times 1.25^{\circ}$) along with masks in the various experiments to follow. We are in no way intending to depict state boundaries in this figure, nor do we imply that what we describe as South Asia represents all countries within that political region.

Table 1 Summary of experiments perturbing the Indian land surface in MetUM GA3/GL3, each for 1983-2002 using AMIP forcing. The perturbation regions are as shown in Fig. 3. References to the land surface and orography apply to the region of perturbation only. Lake depths are 5m unless otherwise stated.

name	region of perturbation	surface conditions	orography
control	–	standard	✓
no_pen	peninsula (removed)	sea	✗
lake_pen	peninsula	lake	✓
bare_pen	peninsula	bare soil	✓
orog_no_pen	peninsula (removed)	sea	✓
no_orog	peninsula	standard	✗
lake_IGP	Indo-Gangetic Plains	lake	✓
lake_SA	South Asia	lake	✓
no_SA	South Asia (removed)	sea	✗
lake_pen50	peninsula	lake (50cm)	✓
lake_pen5	peninsula	lake (5cm)	✓

Where appropriate, statistical testing on the difference between sample means is performed using a student's t-test.

Main experiments - role of the peninsula

In the first experiment, we test the role of the Indian peninsula itself by removing the topography from the model. This involves changing all land points in peninsular India to sea, thus altering the land-sea mask and land fraction configurations of the model. The peninsula is removed south of 22.5°N such that an approximately zonal line can be drawn across from the northern coast of the Arabian Sea to that of the Bay of Bengal. This is known as the *no_pen* experiment.

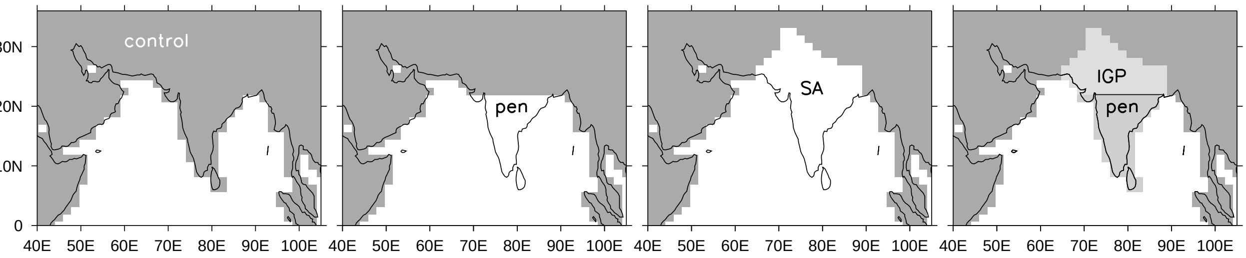

Fig. 3 Land-sea masks at the model N96 resolution (1.875° × 1.25°) in (a) *control*; (b) *no_pen*; (c) *no_SA* experiments; and (d) depiction of the peninsula and Indo-Gangetic Plains. We are in no way intending to depict state boundaries.

Orography is also removed and values for other fields dependent on the land surface such as vegetation are blanked out. Next to be resolved is the forcing at the lower boundary, in the sea points where the peninsula used to be. Atmosphere-only integrations of GCMs derived CMIP-class models (Meehl *et al.*, 2007; Taylor *et al.*, 2012) are typically forced with AMIP sea surface temperatures (SSTs) made available by the Program for Climate Model Diagnostics and Intercomparison (PCMDI). Since many models operating at the same resolution have different ways of representing coastlines, the AMIP forcing SST dataset is made available covering all points on the globe, even beneath the land. The SSTs beneath the land regions are based on interpolation between adjacent seas. Clearly such interpolations over the large land masses such as Eurasia or Africa would be meaningless, but interpolating underneath India between the Bay of Bengal and Arabian Sea we feel will offer SSTs that would be reasonably 'representative' should the peninsula not, in fact, exist. Figure 4 shows the daily seasonal cycle of SSTs applied beneath the removed points of the Indian peninsula averaged

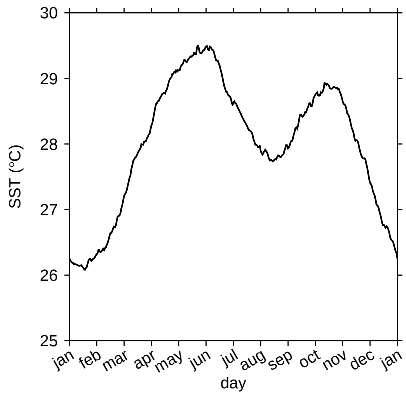

Fig. 4 Daily seasonal cycle of prescribed SSTs in the *no_pen* experiment, area-averaged over grid points beneath the peninsular land surface south of 22.5°N and meaned over 1983–2002. Units are °C.

over the 1983–2002 experimental period. The twin peaks are rather similar to those in the Arabian Sea (Ju and Slingo, 1995), representing late spring warming, cooling due to strong monsoon winds and then, as these winds weaken, some final warming prior to the onset of winter as the Sun moves south of the equator.

To further determine the role of the peninsula on the maintenance and onset of the monsoon in MetUM GA3/GL3, we perform experiments in which the Indian land surface conditions are perturbed. We start from two experiments, *lake_pen* and *bare_pen* respectively, in which the peninsula (south of 22.5°N) is replaced by 100% inland lake or 100% bare soil respectively, representing extremes of the possible land surface tiles available in the JULES land surface model. In *lake_pen* we are effectively offering an unlimited supply of moisture at the surface, rather like the *no_pen* experiments. The temperature of the inland lake tile is controlled by radiation and turbulent heat fluxes at the surface, acting on a heat capacity set by assuming an effective depth of $d = 5$m. In *bare_pen* we are obviously limiting the supply of moisture to the atmosphere through evapotranpiration from the surface. Both will have an impact on surface roughness.

Role of orography

In *orog_no_pen* we exploit a quirk of the model functionality in which it is possible to maintain orography over regions of sea. The *orog_no_pen* experiment is set up in the same way as *no_pen*, except the orography over the peninsula is still present. This mainly constitutes the Western Ghats, the narrow range of mountains on the west coast of India responsible for much orographic rainfall and part of the regional rainfall distribution over the peninsula (Turner and Annamalai, 2012). We prescribe the same SSTs as in *no_pen* and do not allow for lapse rate with height. In *no_orog* we maintain the Indian peninsula but simply remove the orography by flattening the Western Ghats, to test the role of the mountains separately.

Role of the Indo-Gangetic Plains

Further variations on *no_pen* are performed to test the role of the Indo-Gangetic Plains. In *no_SA*, we remove the land points approximating all of South Asia (SA hereafter), all the way to the Himalayan foothills. This was achieved by extending the sea region in the *no_pen* experiment northwards such that all regions of orography less than 750m height were converted to sea points, thus encompassing the Indus and Ganges basins. Note that we are explicitly not intending to address the issue of the role of the movement of the Indian tectonic plate and resultant Himalayan/Tibetan Plateau uplift on the monsoon.

The relative role of heat capacity and moisture availability

Our final experiments adjust the effective lake depth to test the relative role of heat capacity and moisture availability. While we have set the surface heat capacity in the *lake_pen* experiment to give an effective depth of 5m, we reduce this heat capacity by 10× and 100× to give effective depths of 50cm and 5cm in *lake_pen50* and *lake_pen5* respectively. This will allow us to gauge the effect of heat capacity on the diurnal cycle of surface fluxes and boundary layer evolution.

3 Results

3.1 Removal of the peninsula and the role of orography

Here we describe the results of experiments in which the peninsula of India is removed, and its effect on the subsequent summer monsoon. The main impact of removal of the peninsula on the precipitation and flow of the South Asian monsoon is shown in Figure 5. In comparison to the *control* integration, the monsoon climate of *no_pen* in Figure 5a suggests rather more rainfall over central and eastern India and less divergence of the flow around the region of the Western Ghats. In Figure 5b, this result is confirmed and there is a clear cyclonic/anticyclonic anomaly from north to south over the peninsula. In addition, there is a large and significant increase in monsoon rainfall in the southwest Bay of Bengal. The extension of the northeasterly flow anomaly from the south of India and Sri Lanka into the Bay of Bengal results in substantially reduced rainfall over Burma and Bangladesh, as less moisture is being advected there. At first glance therefore, the presence of the Indian peninsula appears to weaken the monsoon over India.

It should be noted that removing the Indian peninsula and getting what appears to be a stronger monsoon is not in itself surprising. The idea of a simple land-sea contrast between the peninsula and surrounding seas in initiating and maintaining the Asian monsoon is an obvious over-simplification. As shown in Turner and Annamalai (2012), the temperature gradient exists over a much larger meridional scale: from the relatively cold southern Indian Ocean high pressure region to the intense heating over the Tibetan Plateau (Li and Yanai, 1996). An atmospheric GCM has also been used to show the importance of the Himalaya in restricting the advection of dry air into the monsoon domain (Boos and Kuang, 2010). Both the Himalaya and Tibetan Plateau are unperturbed in our *no_pen* experiment, in contrast to the experimental design in other studies.

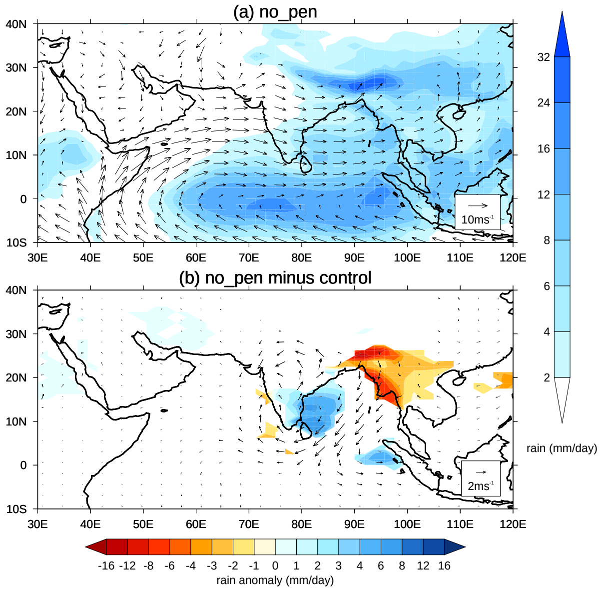

Fig. 5 Summer (JJAS) monsoon climate in the (a) *no_pen* integration showing daily mean precipitation and lower tropospheric (850hPa) winds; and (b) differences between *no_pen* and *control*. Wind field is shown by gray vectors; wind differences significant at the 95% level using a student's t-test are shown in black. Only precipitation differences significant at the 95% level are shown. Units are mm day^{-1} and ms^{-1} respectively.

In removing the peninsula, clearly we have perturbed several aspects of the topography, primarily including the orography (the Western Ghats) and in providing an unlimited supply of moisture at the surface. The moisture will act to feed additional rainfall in addition to that advected across from the Arabian Sea and southern Indian Ocean. Next we explore further the role of the orography, with experiments where the orography is removed (*no_orog*).

Orography

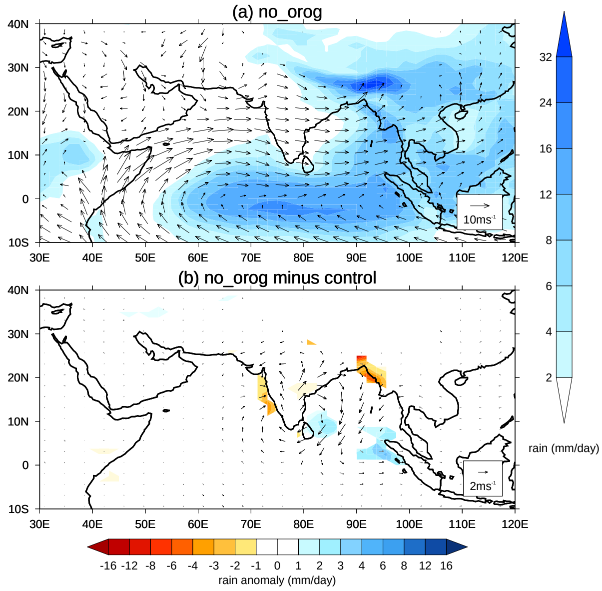

Fig. 6 Summer (JJAS) monsoon climate in the (a) *no_orog* integration showing daily mean precipitation and lower tropospheric (850hPa) winds; and (b) differences between *no_orog* and *control*. The wind field is shown by gray vectors; wind differences significant at the 95% level using a student's t-test are shown in black. Only precipitation differences significant at the 95% level are shown. Units are mm day^{-1} and ms^{-1} respectively.

Given the strong apparent influence of the Western Ghats as part of the orography of the Indian peninsula on the monsoon in Figure 5, here we examine the role of orography explicitly. Figure 6 shows the impact of removing the orography of the peninsula (but maintaining the land surface) on the monsoon climate. Rather similar to the anomalous flow pattern shown in Figure 5b, Figure 6b illustrates that without the Western Ghats present, flow speed is increased at around 18°N (roughly the centre of the west coast) by around 2ms^{-1}. This leads to an cyclonic/anticylonic anomaly in the meridional direction. The anticyclonic anomaly to the south leads to anomalous north-easterly flow across the Bay of Bengal, opposing the mean monsoon flow and reducing rainfall along the Burmese coast. As expected, there is also reduced orographic precipitation just off the west coast of India; in consequence the rain shadow region over southeast India and Sri Lanka becomes wetter.

Part of the signal illustrated in Fig. 6b can clearly be explained by the influence of the Western Ghats perturbing the low-level flow. The Western Ghats add a southerly component to the flow, which would otherwise be zonal across the Bay of Bengal (Fig. 5a). This is consistent with the arguments of Slingo *et al.* (2005), who removed the East African Highlands in the HadAM3 GCM to show that they introduced a meridional component to the flow in the Arabian Sea, Bay of Bengal and South China Sea. It appears the Western Ghats are instrumental in aiding this flow in the Bay of Bengal, with a consequent vital role in precipitation distribution on the west coast of the Indochina peninsula.

In summary therefore, the presence of the Western Ghats seems to slow the monsoon flow and increase upstream rainfall.

We also tested the role of parameterized sub-gridscale orography in a separate experiment (not shown), where measures of the gradients and standard deviations within the grid square were set to zero, while the mean orographic height was maintained. This was found to have no significant impact on the circulation or rainfall. Results of the *orog_no_pen* experiment (not shown), in which the Western Ghats are retained over a sea surface, are similar to those of *lake_pen* but larger in magnitude (see Fig. 7b in the following section). This is probably as a result of changes in the diurnal cycle (see later). We next investigate what role the land surface plays in the monsoon.

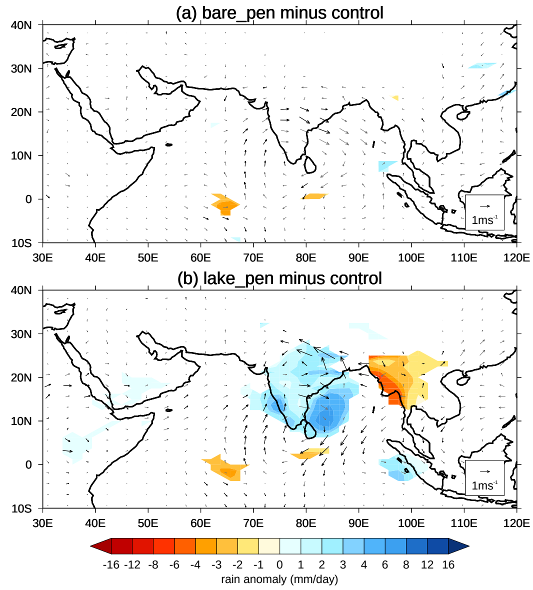

Fig. 7 Summer (JJAS) monsoon differences from the *control* integration in (a) *bare_pen* and (b) *lake_pen* integrations showing daily mean precipitation and lower tropospheric (850hPa) winds. The wind field is shown by gray vectors; wind differences significant at the 95% level using a student's t-test are shown in black. Only precipitation differences significant at the 95% level are shown. Units are mm day^{-1} and ms^{-1} respectively.

3.2 Perturbing Indian land surface conditions

Here we describe experiments where the land surface type over the Indian peninsula is perturbed: in *bare_pen* and *lake_pen*, where the land surface type is set to 100% bare soil or inland lake respectively.

Figure 7 shows the impact of 100% bare soil or inland lake in the peninsula on monsoon rainfall. There is little impact of the *bare_pen* experiment (Fig. 7a) on the monsoon, as witnessed by the absence of signal in precipitation over India. Since the introduction of bare soil reduces the capacity of the land surface to hold soil moisture but greatly reduces roughness length, then we may expect sensible heat from the surface to increase and latent heat to decrease (see later for more detail), both of which would act to restrict monsoon rainfall. Since rainfall over central India is rather low in the *control* however, it is unlikely to be reduced further. Using the HadGEM2 model in atmosphere-only configuration, Martin and Levine (2012) showed that bare soil over India generates dust that tends to reduce rainfall through its radiative effects. Although increased dust loading is also seen in our experiments, the impacts on rainfall are minimal because there is already very little rainfall in this region in the control. Unlike precipitation, the flow is shown to increase, implying increased convergence over the peninsula. This is likely driven by the reduced surface roughness and increased surface heating. Thus the implication is that the roughness of the normally-vegetated surface decelerates the flow across the peninsula.

Figure 7b demonstrates that *lake_pen* has a much more dramatic impact on the monsoon climate, with the strongest increase yet in the rainfall. Significant increases in precipitation of up to 6mm day^{-1} are noticed over the peninsula, with maxima over the west coast and in the north-east (suggesting that monsoon depressions may be playing a role (see later). Increases of up to 8mm day^{-1} are also found over the southwest Bay of Bengal. There are also statistically significant changes to the monsoon flow, which over India may relate to the decreased roughness length as in Fig. 7a. The southwesterly anomalies at the south of the west coast of India act to turn the mean flow northwards slightly and are likely a response to the increased rainfall. The increased strength of the monsoon trough is reflected in the increased strength of south-easterlies there. There is also some evidence for anomalous flow away from the Burmese coast, explaining the reduced orographic rainfall there. Over the western equatorial Indian Ocean there are significant reductions in rainfall of up to 4mm day^{-1}, helping reduce the bias (Fig. 2). There is a considerably larger region of rainfall decrease below the 95% significance level (not shown).

As stated in Section 2.1, the dominant initial land use class in MetUM GA3/GL3 is C3 grasses and thus the transformation to inland lake both decreases roughness length and provides an essentially unlimited supply of moisture at the surface. Both these factors, as we shall see later, increase the flux of latent heat from the surface leading to an increase in moisture in the boundary layer. To put another way, the normal surface of India thus serves to increase roughness length and decrease the availability of moisture. While we will look into more detail of the mechanisms involved in Section 5, first we further explore the importance of the Indo-Gangetic Plains region (which coincides with the monsoon trough) in experiments where low-lying regions of South Asia north of 22.5°N (*lake_IGP*) and the whole of the South Asian subcontinent (*lake_SA*) are covered in lake.

The role of the Indo-Gangetic Plains

To elucidate the impact of unlimited moisture availability at the Indian land surface further, we describe here the results of experiments where surface conditions are changed in the Indo-Gangetic Plains (IGP) region. The *lake_IGP* and *lake_SA* experiments, in which either the Indo-Gangetic Plains only or the whole of South Asia up to the Himalayan foothills are covered in 100% lake respectively, or *no_SA* where South Asia is removed completely, are compared with the *control*. Regions used are as in Fig. 3. The Indo-Gangetic Plains are particularly interesting owing to their proximity to the

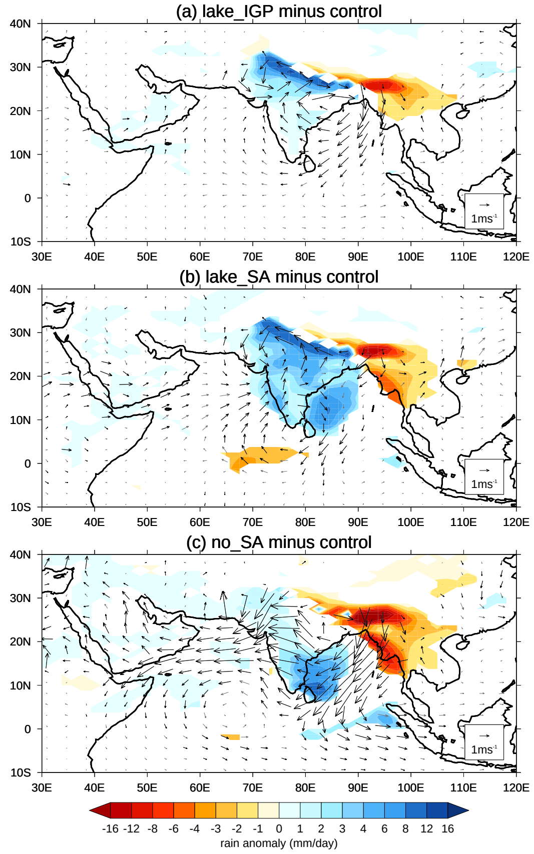

Fig. 8 Summer (JJAS) monsoon differences from the *control* integration in (a) *lake_IGP*, (b) *lake_SA* and (c) *no_SA* integrations showing daily mean precipitation and lower tropospheric (850hPa) winds. The wind field is shown by gray vectors; wind differences significant at the 95% level using a student's t-test are shown in black. Only precipitation differences significant at the 95% level are shown. Units are mm day^{-1} and ms^{-1} respectively.

monsoon trough, the widespread use of irrigation for agriculture and its characterisation as a global hotspot of land-atmosphere coupling (Koster *et al.*, 2004). The high resolution and more detailed classification NRSC/AwiFS data mentioned in Section 2 shows much of the plains to consist of irrigated cropland or pasture.

We first look at the Indo-Gangetic Plains in isolation (*lake_IGP*) in Fig. 8a. There is a clear shift of precipitation from the Himalaya to the foothills region and the Indo-Gangetic Plains. Since the response of the flow is mainly recirculating within the region and not advecting additional moisture from either the Arabian Sea or Bay of Bengal to this region, the increase must comprise increased local evaporation. This is consistent with results of Tuinenburg *et al.* (2012) who noted that 60% of summer surface moisture in the Ganges region was recycled into the atmosphere. The increase in precipitation of 12mm day^{-1} or more underlines the sensitivity of the monsoon to land surface configuration changes here (see the land-atmosphere coupling hotspot in Koster *et al.*, 2004). We will see later the separate impacts of heat capacity and water availability in the lake experiments. Although our examination is idealised, this may have implications for the expansion of irrigation practices for agriculture (Niyogi *et al.*, 2010) including the use of tube wells and other forms of groundwater extraction making available hitherto untapped water to the atmosphere. Saeed *et al.* (2009) also showed using the REMO regional model that allowing evaporation to increase to the maximum potential evapotranspiration rate in regions of strong irrigation (mainly in the northern plains) led to a strong increase in local recycling.

Looking more widely at the *lake_SA* experiment, Fig. 8b shows a rainfall and circulation response that seems to be a magnification of the *lake_pen* experiment shown in Fig. 7b. It features a significant enhancement of the Somali jet across the Arabian Sea and rainfall increase by at least 6mm day^{-1} in the far north of the domain up against the Himalayas. The western Bay of Bengal also features increases in rainfall as in the *no_pen* and *lake_pen* experiments.

To complete the picture, Fig. 8c shows the results of the *no_SA* experiment, in which the South Asia region is replaced by sea surface. The response now is more complex. This experiment differs from *lake_SA* not only in the lack of feedback on surface temperatures but also in having no orography. The precipitation signal shows increases centred on the southwest Bay of Bengal, as in *no_pen* but also in the same position as one of the large signals in *lake_pen* and *lake_SA*. However, unlike those other experiments, there is a clear weakening of the monsoon circulation, especially in the northern Arabian Sea but even extending to the cross-equatorial part of the flow. To understand these more nuanced changes in the monsoon precipitation and circulation, we show the monsoon onset period (June) mean surface temperature and mean sea-level pressure climatologies in Fig. 9.

The *control* (Fig. 9a) shows an elongated trough that extends quite far south in eastern India and reaches as low as 996hPa over the northern plains of India. Experiments in Fig. 9b,c,e all show an intense trough reaching 1000hPa or less, reflecting the strong gradients in surface temperature as we approach the Himalayas from the south. In *no_pen* for example (Fig. 9e), there exists a strong gradient between the sea at around 10°N and the warmer land surface of the Indo-Gangetic Plains, supporting the low-level monsoon circulation. Evidence suggests that surface temperature gradients in the northern Indian Ocean are important in monsoon rainfall (e.g. Chung and Ramanathan, 2006). In *lake_SA* (Fig. 9d), the trough is not as intense as in other experiments (reflecting the weakened surface temperature gradient) but it still falls to 1001hPa. An interesting feature of *lake_IGP* (Fig. 9b) is that it features a maximum in surface temperature on the peninsula while being colder to the north and south. This alters the shape of the trough, weakening it at the head of the Bay of Bengal. The local temperature gradient along the Himalayan foothills when the IGP region is covered in lake seems to drive extra convergence and rainfall there.

When we remove the whole of the South Asia region as in *no_SA* and replace it with sea (Fig. 9f), we considerably weaken the surface temperature gradient as the Himalayas are approached from the south. The maximum in underlying surface temperature forcing extends across from India into the southwest Bay of Bengal, colocated with the maximum increase in rainfall. The reduced temperature gradient has the effect of weakening the monsoon trough, even splitting the low in the northern plains from the strong heat low over southern Pakistan and Iran (from around 60°E), and it only reaches 1003hPa at its lowest. While the overall monsoon circulation does not collapse, the flow especially

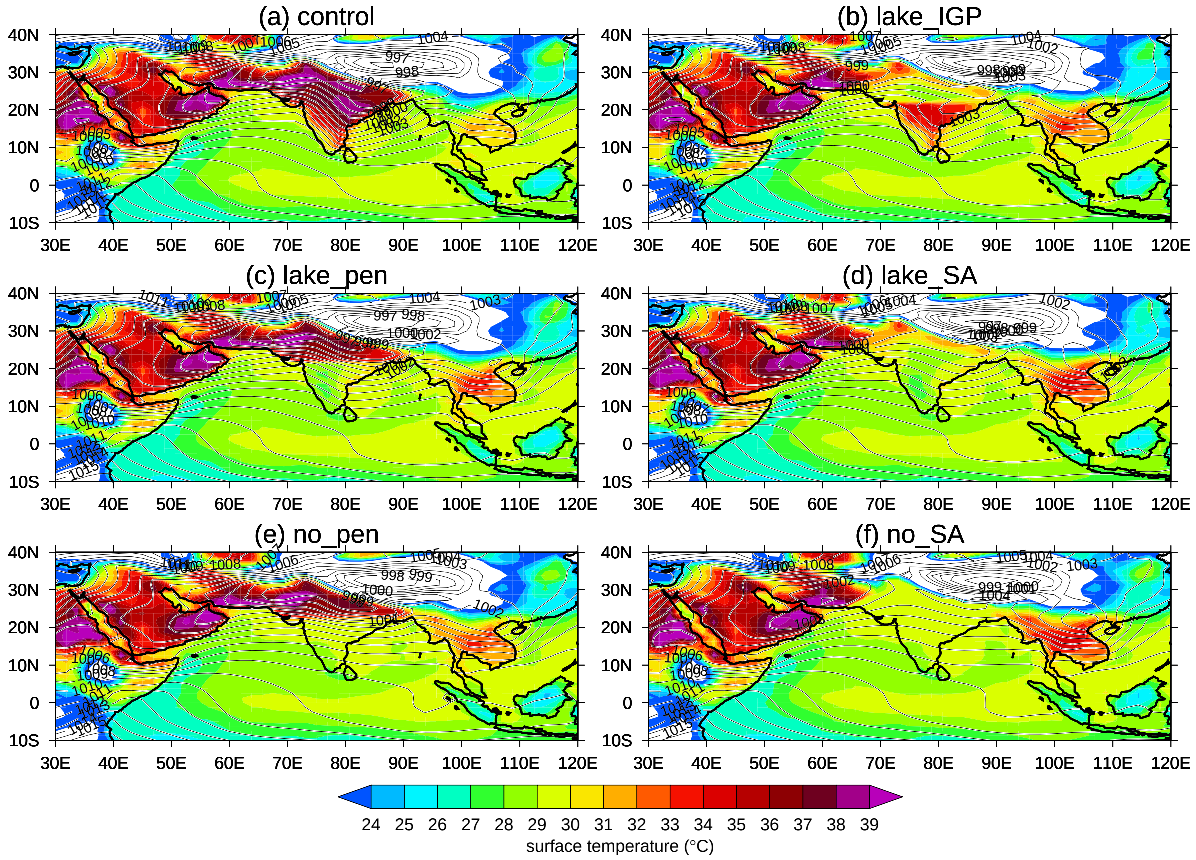

Fig. 9 June average surface temperature (shaded) and mean sea-level pressure (contour lines) in the *control*, *lake_IGP*, *lake_pen*, *lake_SA*, *no_pen* and *no_SA* experiments. Low temperatures over the Tibetan Plateau are omitted in order to restrict the range of the colour scale. Units are °C and hPa. We remind the reader that the Indian coastline is not present in the *no_pen* and *no_SA* experiments.

in the northern part of the Indian Ocean domain is considerably weakened (the circulation anomalies we see in Fig. 8c). This is why the monsoon precipitation does not increase as strongly in *no_SA* as in *lake_SA*.

Hence this section emphasizes the dual but competing impacts of the peninsula in terms of offering a temperature and pressure gradient to sustain the monsoon circulation so far north and that of the moisture availability depending on the surface conditions. We next examine the synoptic and intraseasonal variability in those experiments where rainfall is increasing strongly.

4 Synoptic and intraseasonal variability

4.1 Monsoon depressions

Since much rainfall in northeast peninsular India and the monsoon trough comes from monsoon depressions (Krishnamurthy and Shukla, 2007), here we perform analysis to determine if any of the additional monsoon rainfall noted in the wet surface experiments is coming from greater prevalence of depressions in the region. We examine the *no_SA* and *lake_SA* runs in comparison with the control integration. We don't examine the *lake_pen* or *no_pen* experiments in this context since the imposition of the surface perturbation south of 22.5°N introduces an artificial cut-off through the monsoon trough region, where depressions may be expected to pass.

Analysis is performed using a tracking algorithm (Hodges, 1994) on 6-hourly 850hPa relative vorticity. The data are first filtered to T42 resolution (approximately 2.8° in latitude and longitude). Systems that exceed a vorticity threshold of $5\times10^{-5}\mathrm{s}^{-1}$ for at least 3 days and that travel a minimum distance of 5° are diagnosed. Further, to affect South Asia in a meaningful way the system must spend at least 60% of its lifetime in the 70–95°E, 10–30°N domain. Depression rainfall is estimated in a box approximately 20° around each system.

Figure 10 shows the average summer rainfall in those years in which depressions are diagnosed in *control*, *no_SA* and *lake_SA*. The depression tracks and average rainfall associated with those depressions are shown in the middle column (note that there may be more than one depression per year), and on the right the average rainfall without the influence of monsoon depressions is shown.

In the control integration, the only track diagnosed is short and has only a small area of rainfall associated with it. The number of tracks increases to seven and nine depressions in the *no_SA* and *lake_SA* experiments respectively, over six and seven years. The resulting impact of these depressions on mean precipitation is also larger. We note that in *lake_SA*, depressions tend to be generated near the head of the Bay of Bengal and track along the monsoon trough south of the Himalayan foothills as is typical in observations (see, e.g. Annamalai *et al.*, 1999, Figs. 16 & 17). More detailed examination of individual tracks confirms this (not shown). However in *no_SA* depressions tend to form near the south Bay of Bengal, quite unlike observations, and track northwards as they reach the position of the peninsula. This is consistent with the main change in the mean precipitation as shown in Fig. 8c, and relates to the underlying surface temperature structure: *no_SA* features a maxima in the southwest Bay of Bengal (see, e.g., the June SST distribution in Fig. 9f) and a weak surface pressure gradient and monsoon trough.

Thus the role of the IGP part of the peninsula, if sufficient moisture is available, is in steering monsoon depressions along the monsoon trough (established via surface temperature and pressure gradients) concentrated in the northern plains.

4.2 Northward propagating modes

While we have already shown an increase in activity at the synoptic scale of monsoon depressions, here we briefly describe the occurrence of northward propagating intraseasonal modes of variability at South Asian longitudes in a subset

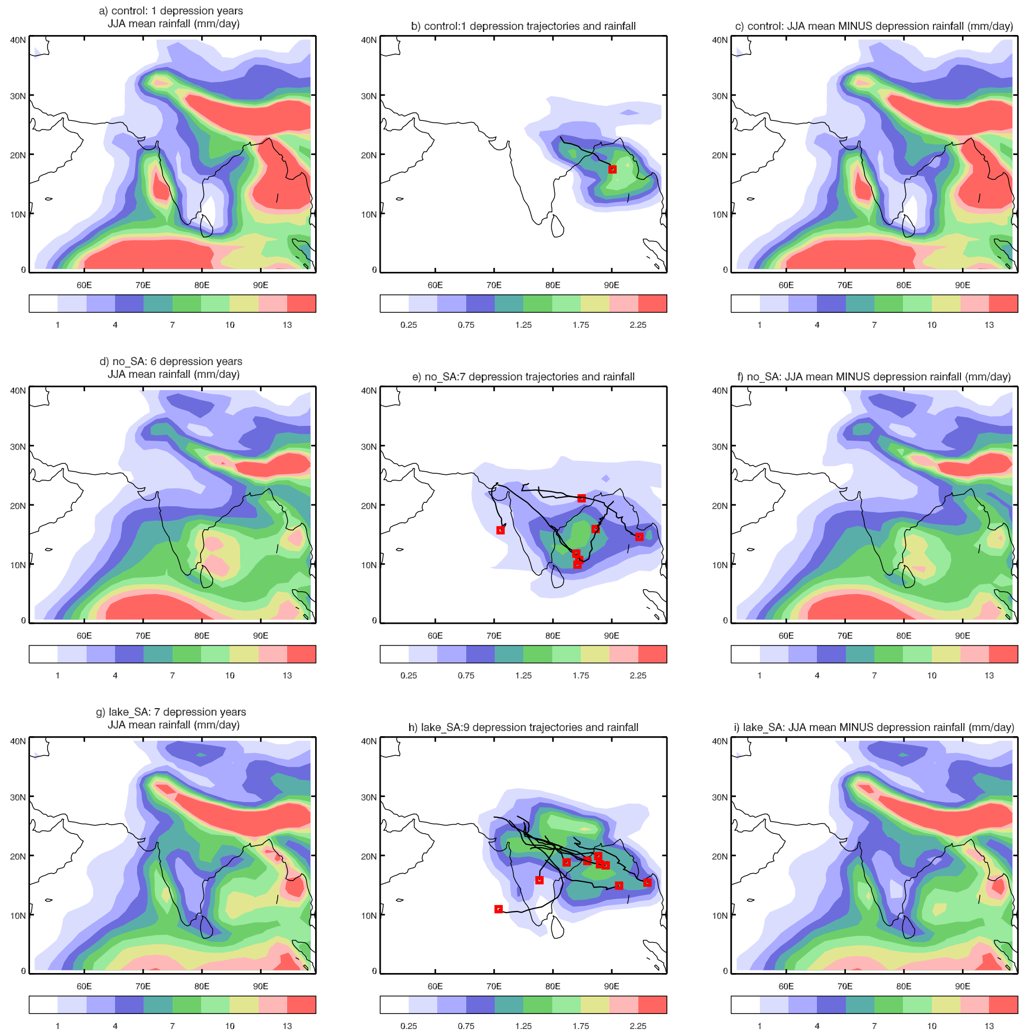

Fig. 10 Analysis of depressions in the monsoon summer (JJA) including (a,d,g) avergage rainfall in years in which depressions are diagnosed; (b,e,h) depression tracks and their associated precipitation; and (c,f,i) average summer rainfall less the contribution from depressions. The *control*, *no_SA* and *lake_SA* experiments are shown. Units are mm day^{-1}. Red squares mark the starting points for each depression.

of the experiments. We calculate lag-correlations of precipitation, band-passed into 30–60 day periods using a Lanczos filter (Duchon, 1979) and averaged over the 70–100°E range of longitudes with precipitation at a point in the Bay of Bengal near 12.5°N, 85°E after Turner and Slingo (2009); Lin *et al.* (2008) and others. Figure 11a shows good evidence for northward propagation in GPCP precipitation observations, but only weak evidence in the *control* integration. Weak northward propagation is also detected in *bare_pen* (not shown). In the experiments in which we wet the surface and precipitation is enhanced over the peninsula region (*lake_pen* and *no_pen*), there is clear evidence of more coherent northward propagating modes of intraseasonal variability, although at slower phase speeds than in observations. In

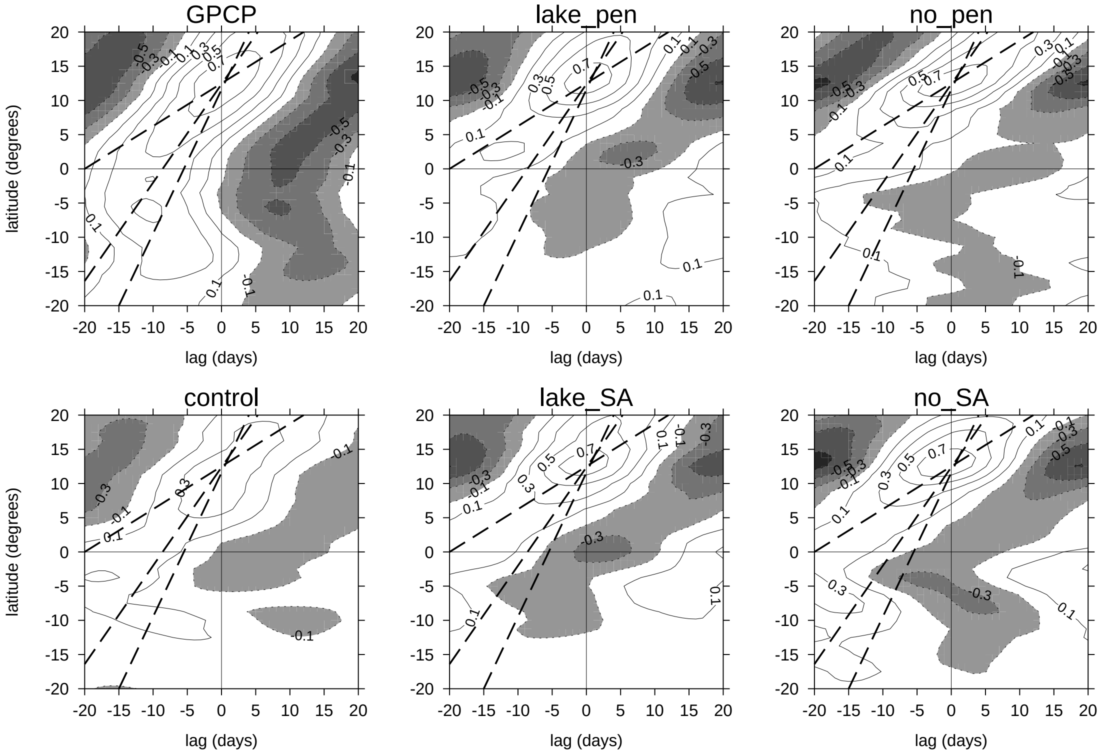

Fig. 11 Lag-correlations of 30–60 day bandpass-filtered precipitation averaged over the 70–90°E band against precipitation at 12.5°N, 85°E in GPCP observations and model experiments after Lin *et al.* (2009). The *control*, *lake_pen*, *no_pen*, *lake_SA* and *no_SA* experiments are shown. The dashed straight lines show phase propagation speeds of 0.8, 1.8 and 2.8ms^{-1} respectively.

the experiments in which we wet the surface of the whole of South Asia (*lake_SA* and *no_SA*), results are also consistent with the above. Interestingly, in the *no_pen* and *no_SA* experiments there is also the suggestion of southward propagation from the equator as in observations, although we do not know the cause of this. When we cover the Indo-Gangetic Plains only with water (*lake_IGP*), little notable difference is made to the propagation (not shown), possibly because we are not changing the existing temperature gradient between the peninsula and ocean, which may play a role in drawing convection northwards on intraseasonal time scales.

The results here and in the previous section discussing depressions suggest that much of the increased precipitation is associated with organised systems. So the presence of the peninsula (in this model) reduces the occurrence of organised systems but acts to locate them in the trough region. The latter may be a ‘real’ effect while the former *may* be an artefact of model bias.

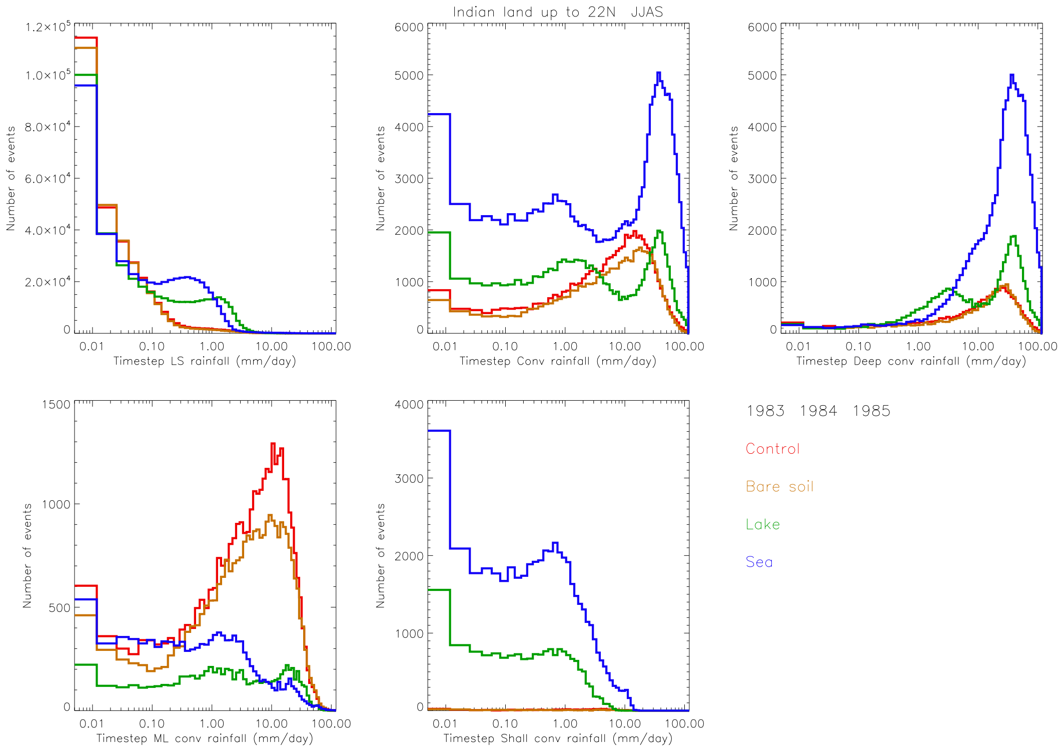

Fig. 12 Histograms showing summer (JJA) precipitation rates measured at every time step and each grid point over the Indian land region south of 22°N. The *control*, *bare_pen*, *lake_pen*, and *orog_no_pen* experiments are shown with precipitation from (a) the large-scale (LS) precipitation scheme and (b) convection scheme; the latter split into (c) deep; (d) mid-level and (e) shallow convection components. Note the log scale on the $x-$axis.

5 Convective, diurnal cycle and boundary layer processes

5.1 Time-step analysis of changes in rainfall

Here we describe how changes to precipitation have occurred at the time-step level including the intensity of precipitation and the type of convection diagnosed by the convection scheme in MetUM GA3/GL3. We take model output from individual time steps ($\Delta t = 1200$s) for three summers only, due to the computational expense of outputting these data.

In Fig. 12 we show histograms of time step precipitation over land grid points south of 20°N split into that produced by the large-scale scheme and by the convection scheme separately. The convective precipitation is further split into rainfall diagnosed as shallow, mid-level or deep (see the description in Section 2.1 for more details). For consistency, all the integrations compared contain orography.

Rainfall diagnosed by the large-scale scheme is extremely common at very low rain rates (0.01mm day^{-1}), suggesting that drizzle is occurring unrealistically on some grid points over the peninsula region at all times. At rain rates >0.1mm day^{-1}, there is a clear separation between the experiments, with there being a noticeably higher number of large-scale events in the runs with sea (*orog_no_pen*) or lake (*lake_pen*) present at the surface. There is little difference between the *bare_pen* and *control* experiments here or in most of the other time-step analysis, consistent with the lack of precipitation difference caused by imposing bare soil at the surface (see Fig. 7a).

Convective rainfall, which makes up the majority of rainfall above negligible rain rates in the tropics, seems to be made up of contributions in shallow convection at the lowest rates and mid-level and deep convection at the higher rates. However the surface type makes a clear difference here. The biggest change in the spectrum comes from changes from normal land to lake or sea, with large increases in the frequency of deep convection at around 30mm day^{-1} (more so for the *no_pen* rather than *lake_pen* surface). For mid-level convection, there is a far lower contribution when there is lake or sea at the surface, reflecting a shift in the balance between deep and mid-level convection in these experiments. The presence of deep lake or sea at the surface with inherent high heat capacity prevents the boundary layer becoming stable at night, allowing the dominance of deep convection. Moving from land to water at the surface also shifts the spectrum of shallow and mid-level convection to lower rain rates. The overall contribution of shallow convection at meaningful rain rates is small so we shall not discuss it here, although again the difference is probably also due to the change in diurnal cycle.

It is important to note that the sensitivity shown here may be exaggerated by the model framework, owing to the influence of the relatively coarse resolution of current GCMs and associated deficiencies in convective parameterisation. The time-step analysis in *control* suggests that in the model most land rainfall is generated from local diurnally-forced convection and not from organised systems (see also analysis of monsoon depressions earlier and our later analysis of the boundary layer). Observational evidence (Krishnamurthy and Shukla, 2007) suggests that organised systems make up much of the rainfall especially over northeastern peninsular India. As we shall see later, the diurnal cycle over the land surface (controlled by the surface heat capacity) also plays a role in the occurrence and type of convection.

Analogous analysis in the runs with no orography present (not shown) indicates that the presence of orography mainly adjusts the relative heights of the peaks of deep convection. In the absence of orography, the sea surface features a much reduced count of deep convective events at around 30mm day^{-1}.

We next explore the seasonal and diurnal evolution of surface fluxes and the boundary layer.

5.2 The seasonal cycle at the surface

Here we go into further detail surrounding the mechanisms involved at the surface and in the planetary boundary layer in some of the experiments outlined above. For brevity, in most parts of the analysis we consider only the comparisons of *lake_pen*, *bare_pen* and *no_pen* with the *control* integration. We first examine the turbulent heat fluxes from the surface (sensible and latent heat) as components of energy input to the atmospheric column, as shown in Fig. 13a. The *control* run shows the dominance of sensible over latent heat fluxes at the surface (hence a Bowen ratio exceeding unity). A similar result is seen in *flat_pen*, illustrating the overriding influence of the land surface type over these fluxes, rather than the circulation changes perturbed by orography, which occur only over a small part of the peninsula (Fig. 6b). In *bare_pen* the total sensible and latent heat fluxes fall slightly. This shows that the presence of vegetation over the peninsula increases the Bowen ratio. In the experiments with water at the surface, sensible heating falls to low values, while latent heating dominates. In *lake_pen* this has a strong seasonal cycle, reflecting the supply of moisture made available to the monsoon as the circulation evolves (see the peninsula-average 10m wind speed as in Fig. 13b) and the seasonal cycle of temperature. In *no_pen*, the cycle of latent heating is more complex. Here the winter maximum results from the convolution of the surface wind speed (Fig. 13b), including its peaks for summer and winter monsoons, with the SST field imposed at the surface underlying the Indian peninsula (Fig. 4), which is necessarily driven by the seasonal cycle of SST in the surrounding ocean. The winter monsoon winds are also drier since they originate from over Eurasia, encouraging evaporation and latent heat flux from the surface.

The wind speeds shown in Fig. 13b suggest that the dominant influence on the near-surface winds is due to perturbing the land surface type, with similar reductions in surface roughness in *bare_pen* and *lake_pen* offering similar increases in wind speed during both monsoon seasons. This reflects the standard roughness length for bare soil and lake surfaces of 3×10^{-4}m (Best *et al.*, 2011). The *flat_pen* experiment offers a smaller increase in surface winds; this increase adds approximately linearly to that in *lake_pen* to equal the increased winds speed in *no_pen*, representing the sum of effects due to the land surface change and removal of orography. This implies that the Indian peninsula acts to slow the winds through the effects of surface roughness, especially where vegetation is present, and orography adds to this.

Next we examine the net convergence of heat and radiative fluxes into the atmospheric column (F_{net}), after Chou and Neelin (2003) as shown in Fig. 13c. We sum the input of turbulent heat fluxes at the surface (from Fig. 13a) with the net longwave and shortwave inputs to the atmospheric column at the top of atmosphere (TOA) and surface. We neglect longwave inputs at the TOA as negligible. As in other measures, the net flux of energy into the atmospheric column is unperturbed by the *bare_pen* experiments. The removal of orography in *flat_pen* also has little effect, reflect-

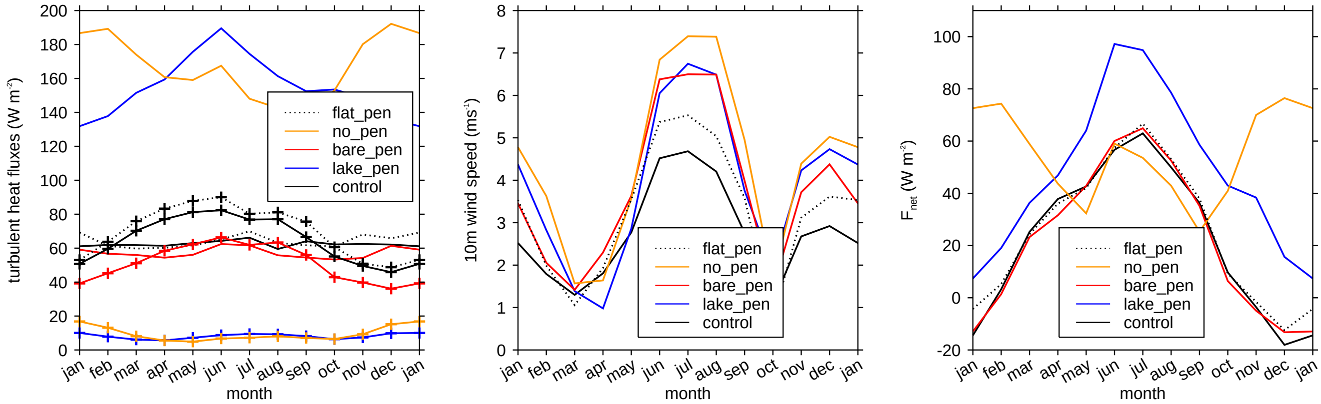

Fig. 13 Monthly seasonal cycle of (a) surface turbulent heat fluxes; (b) surface wind speed (at 10m); and (c) net heat and radiative fluxes into the atmospheric column (F_{net}) including the input of turbulent heat fluxes at the surface and the net longwave and shortwave fluxes at the top of atmosphere and surface, in the *control*, *bare_pen*, *lake_pen*, *no_pen* and *flat_pen* experiments. Area-averaging is performed over all land surface grid points south of 22.5°N. In (a), sensible (latent) heat fluxes are shown by the crossed (straight) lines. Units are W m^{-2}, °C and W m^{-2} respectively.

ing the lack of perturbation to the surface conditions. The change in *no_pen* reflects those in the seasonal cycle of latent heat flux as in Fig. 13a. That it does not increase above the level of *control* in summer reflects the minimal change in precipitation over the peninsular area average region in *no_pen* (Fig. 5b). The experiments with non-saturated surfaces, including *control*, show negative convergence into the column during boreal winter, reflecting the much lower surface temperatures. Most dramatic is the extra convergence of energy into the atmospheric column in the *lake_pen* experiment. Chou and Neelin (2003) have implied that in regions not dynamically ventilated, increasing F_{net} should lead to enhanced monsoon convection. So the increased F_{net} is consistent with the enhanced monsoon convection.

The peninsula therefore acts to fix the seasonality of F_{net}, with the level of moisture at the surface controlling its magnitude.

5.3 The diurnal cycle

Next we look at behaviour at a diurnal level, including surface temperature, turbulent heat fluxes, the boundary layer and precipitation. We first examine the summer diurnal cycle of surface temperature (ST) in the experiments, from 3-hourly averaged output data. We perform the calculation based on all points south of 22.5°N which are (or were) land. Figure 14 shows a large summer diurnal cycle in ST that is exacerbated by changing to bare soil. The strong diurnal cycle is likely excessive owing to the weak rainfall over parts of the peninsula during the monsoon in this model. The *lake_pen* and *no_pen* experiments show very limited and no diurnal cycle in ST, respectively. In *no_pen* there is no diurnal cycle in the prescribed underlying SST and therefore this diagnostic is limited. Similarly in the *lake_pen* experiment, the large surface heat capacity in the 5m lake all but prevents

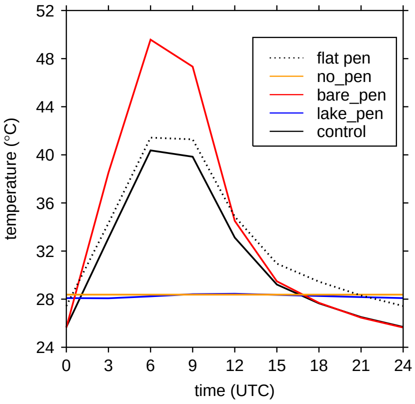

Fig. 14 Summer (JJAS) diurnal cycle of surface temperature using 3-hourly outputs in *control*, *bare_pen*, *lake_pen*, *no_pen* and *flat_pen* experiments. Area-averaging is performed over all land surface grid points south of 22.5°N. Units are °C.

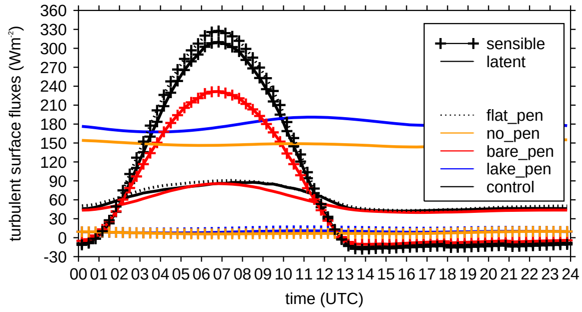

Fig. 15 Diurnal cycle of turbulent surface heat fluxes (latent heat and sensible heat) sampled at each time step and averaged over each grid point of the peninsula south of 22.5°N over JJA of 1983–1985. The *control*, *bare_pen*, *lake_pen*, *no_pen* and *flat_pen* experiments are shown. Units are W m^{-2}.

a diurnal cycle in surface temperature. The sensitivity of this diurnal cycle to lake heat capacity is examined later in this section. There is no significant impact of the orography or lack thereof (not shown).

Following from the diurnal cycle of surface temperature, in Fig. 15 we show the summer diurnal cycles of area-averaged latent and sensible heat fluxes from the surface over the peninsula using timestep data. In the *control* there is a large diurnal cycle in sensible heating consistent with the largely dry surface, peaking around midday local time. The sensible heating becomes negative at night, stabilising the lower atmosphere and representing a key difference between the diurnal cycles over land and water surfaces. The change in orography makes little difference to this field as in the annual cycle in Fig. 13a. The diurnal cycle of latent heat flux (evaporation) is far smaller. In the *bare_pen* experiment, the diurnal cycle of sensible heating is reduced, consistent with the annual cycle in Fig. 13a. The biggest change comes in those experiments where the surface is wet (*lake_pen* and *no_pen*), in which sensible heating is much reduced and stays positive throughout the night, reflecting the very small diurnal cycle of temperature in these experiments while latent heat release is strongly increased. This is reasonably uniform throughout the day reflecting the consistent vapour deficit between the surface and the near-surface atmosphere. The impact of the peninsula is therefore to enhance the diurnal cycle of surface temperature and sensible heat flux at the surface and to reduce the latent heat flux.

Since convection is connected to the surface via the boundary layer, finally we consider boundary-layer behaviour in the experiments. We explore this using time-step outputs from the experiments, as in Section 5.1. To construct Fig. 16 we first compute a mean diurnal cycle of the occurrence of the seven different boundary layer types over each grid point

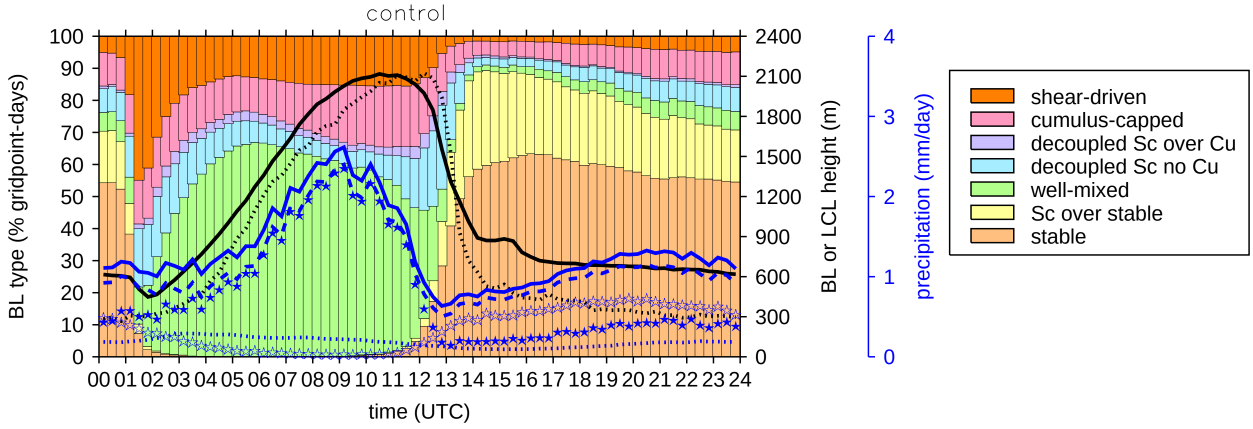

Fig. 16 Stacked bars show the diurnal cycle of proportions of boundary layer types sampled at each time step and averaged over each grid point of the peninsula south of 22.5°N over JJA of 1983–1985 in the *control* run. The average height of the surface mixed layer under stable or well-mixed boundary layer conditions (black solid line) and height of the lifting condensation level during cumulus conditions (black dotted line) are shown on the right axis, units m. Also shown on the far-right axis are the total precipitation (blue solid line) and its convective (blue dashed) and large-scale (blue dotted) components, units scaled to mm day^{-1}. The convective rainfall is further broken down into that arising from deep convection (filled stars) and the mid-level convection scheme (empty stars).

for the summer (JJA) in 1983–1985, then average over the peninsula south of 22.5°N. The temporal resolution is that of the time step: 20 minutes. We remind the reader that local time at Indian longitudes is around 5.5 hours ahead of UTC. For much of the daylight hours, a well-mixed boundary layer dominates, with some cumulus also. Upon nightfall at around 12:30UTC (18:00 local time) the well-mixed boundary layer rapidly diminshes due to the decline in sensible heat fluxes from the surface, being replaced by a stable layer and stratocumulus cloud over a stable layer. At this time the proportion of grid points over which cumulus boundary layers form falls, reflecting the drop in surface-driven deep convection.

In Fig. 16 we also show the mean height of the boundary layer (black solid curve, averaged only when the diagnosed boundary layer type is well-mixed or stable, representing the height of the surface-based mixed layer) and the height of the lifting condensation level (LCL) under cumulus conditions (black dotted curve). There is a clear diurnal cycle in the boundary layer height and LCL, rising during the day due to heat fluxes from the surface and falling rapidly at night to reach as low as 600m.

The diurnal cycle in precipitation (Fig. 16 blue curves) follows a similar evolution, slightly lagging the deepening of the boundary layer. In the *control*, the vast majority of precipitation is convective, and during the day time this is predominantly from deep convection. As the dominant boundary layer becomes stable at night, the majority of convective rainfall is now contributed from the mid-level scheme, because this scheme can operate above well-mixed or sta-

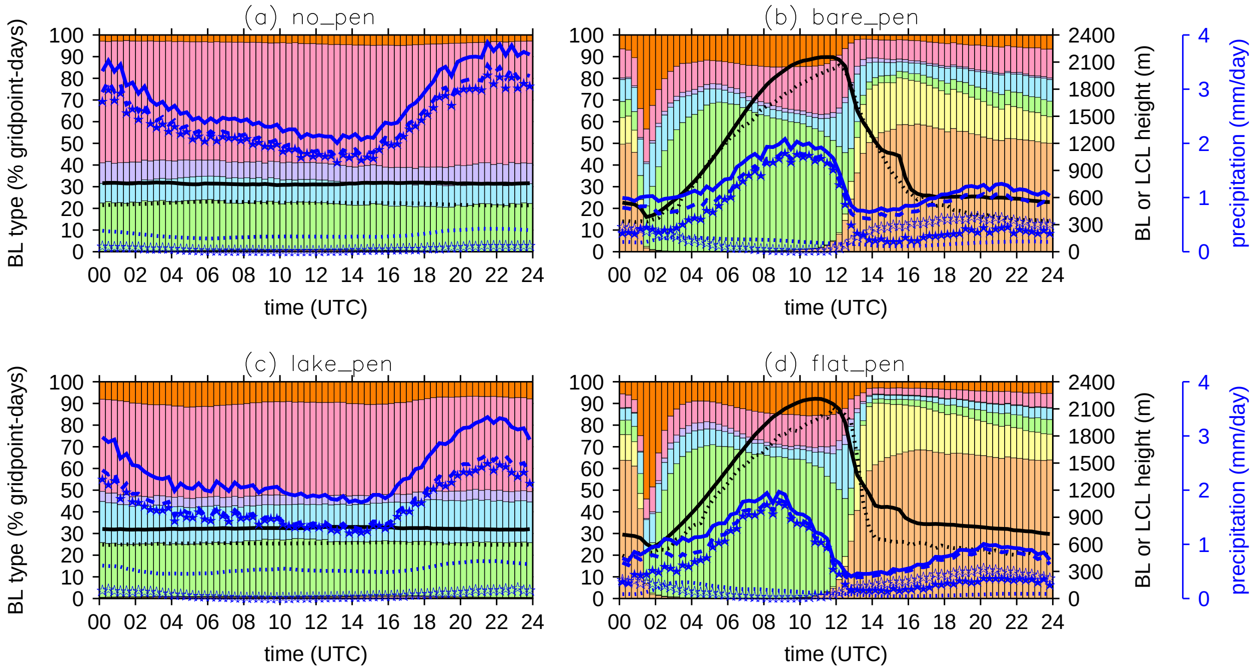

Fig. 17 As in Fig. 16 but for the *no_pen*, *bare_pen*, *lake_pen* and *flat_pen* respectively. Legend is shown in Fig. 16.

ble boundary layers, whereas by definition deep and shallow convection can't.

In Fig. 17 we show the diurnal cycles of the boundary layer in the *no_pen*, *bare_pen*, *lake_pen* and *flat_pen* experiments. Looking at *no_pen* in Fig. 17a, we see a completely different evolution from that in the *control*, with no diurnal cycle in boundary-layer type or depth over peninsular grid points. The cumulus boundary layer type now dominates, in around 40% of cases throughout the day, followed by well-mixed and then decoupled stratocumulus boundary-layer types, the latter both in the presence and absence of cumulus cloud. Stable layers do not develop. The precipitation increase seen in Fig. 5 is composed of increases at all times of day, although it now reaches a maximum in the early hours of the morning rather than the early afternoon as in the control run. This reflects observed diurnal rainfall variability over the ocean, peaking during the nighttime rather than in late afternoon (Bowman *et al.*, 2005). The majority of the precipitation is coming from deep convection, although there is a small proportion (around 0.5mm day^{-1}) from the large-scale scheme.

As earlier in the paper, we now examine the roles of the land surface characteristics and orography on the diurnal cycle of the boundary layer. Figure 17b shows that imposing 100% bare soil in *bare_pen* has little impact on the development of the boundary layer (compared to Fig. 16), in common with the minimal changes in precipitation and circulation shown earlier (Fig. 7a). Further, the removal of orography from the peninsula in *flat_pen* (Fig. 17d alters the boundary layer evolution little. In contrast, imposing 100%

lake at the surface in *lake_pen* (Fig. 17c) leads to most of the change shown by the *no_pen* experiment.

In summary therefore, the presence of the peninsula leads to diurnally forced variations in the boundary layer and convection. These variations are dominated by the stabilisation of the boundary layer at night, which is related to the land surface heat capacity, and the depth of the surface-based mixed layer and height of the LCL during the day, which are related to surface moisture availability and temperature.

Heat capacity versus moisture supply

In our final experiments *lake_pen50* and *lake_pen5* we seek to test the relative role of the surface heat capacity provided by the lake versus that of the additional moisture supplied. The standard *lake_pen* experiment is equivalent to a 5m-deep lake. While we are reducing the effective lake depth globally in these additional experiments (to 50cm and 5cm respectively), since the only expanse of lakes globally is the Great Lakes region of North America, we expect no impact on the South Asian monsoon from these remote regions. The mean changes in the precipitation pattern during JJAS are very similar to those for *lake_pen* in Fig. 7b but are not shown for brevity.

We show the impact on the diurnal cycle of surface temperature data in Fig. 18a. Compared to the near-zero diurnal cycle of the surface in *lake_pen*, the reduced heat capacity of *lake_pen50* and *lake_pen5* progressively enhances the diurnal cycle of surface temperature. This is also clearly reflected in the turbulent surface fluxes of Fig. 18b, which shows a strong diurnal cycle in sensible heating at *lake_pen5*, together with enhanced latent heating throughout the day. Even in *lake_pen50*, sensible heat flux still does not go negative at night, preventing stabilisation of the boundary layer. This allows dual peaks in convective precipitation (blue line in Fig. 18a), corresponding to a combination of typical land and sea diurnal cycles in convection. With a 5cm lake imposed over the peninsula, a strong diurnal cycle in boundary layer activity remains, however the surface-based mixed layer depth and LCL are much lower than in the control, and convective boundary layers dominate over well-mixed layers, allowing for a large mid-afternoon peak in rainfall at a rate of up to 6.5mm day^{-1}. This strong peak makes up for the weaker rainfall at night in contributing to the seasonal mean. Since sensible heat fluxes become negative at night, stable boundary layers dominate.

In summary, the response of the evolution of boundary layer composition clearly suggests that the boundary layer type, and therefore the occurrence of surface-driven deep convection overhead, is highly sensitive to conditions on the surface. The presence of land allows for a large diurnal cycle in surface temperature, surface fluxes and boundary layer stability, and if there is enough moisture available then convective rainfall too. Thus the wet surface experiments show an increase in evaporation during the daytime (and indeed

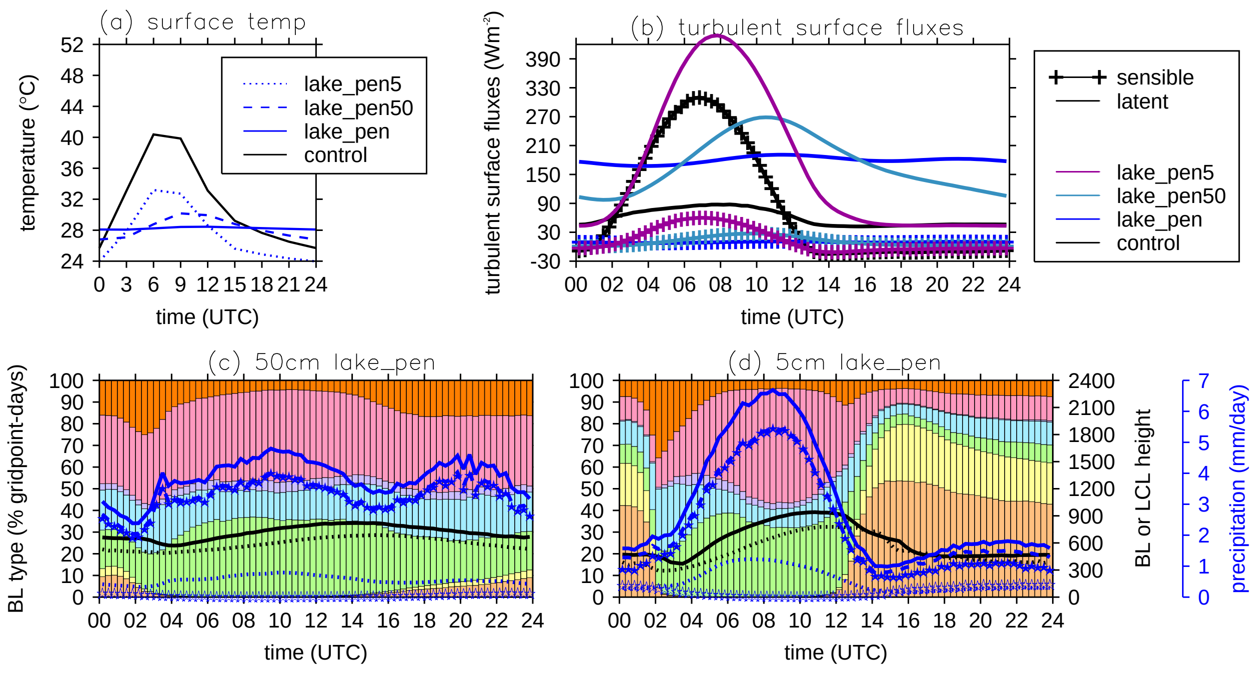

Fig. 18 Diurnal cycles of (a) surface temperature and (b) turbulent heat fluxes as in Figs. 14 and 15; (c) and (d) are as in Fig. 16 but for the *lake_pen50* and *lake_pen5* experiments with 50cm and 5cm depths respectively. Note that the precipitation axis covers a greater range than in Fig. 16.

at night), combined with a much shallower and therefore more moist boundary layer. As the surface heat capacity and effective lake depth increases, the wet surface experiments progressively lead to a more ocean-like diurnal cycle with an additional precipitation peak in the early hours of the morning. If the surface heat capacity is large enough, this ultimately leads to more rainfall at night as shown for the *lake_pen* and *no_pen* experiments. Therefore the impact of having land present is felt partly through the diurnal cycle, itself sensitive to the presence or absence of vegetation and soil moisture. This has implications for models that don't properly represent these characteristics as well as those that have a poor convective diurnal cycle over land.

6 Conclusions

In this study we have examined the role of the broad-scale characteristics of the South Asian peninsula on the Asian summer monsoon in the Met Office MetUM GA3/GL3 land-atmosphere GCM, using a series of novel experiments perturbing the land surface, orography and removing the peninsula itself. The role of the Indo-Gangetic plains region north of the Indian Ocean coastal boundary up to the Himalaya and Hindu-Kush mountain ranges has also been examined.

Initial experiments removing the peninsula south of 22.5°N revealed a pattern of local precipitation and circulation change, increasing the strength of the mean monsoon averaged over the broad South Asia region. Importantly, first-order ideas about the land-sea contrast between the Indian land surface and the surrounding ocean being essential for monsoon development are shown to be simplistic: the large-scale monsoon circulation is still supported when the land peninsula is removed.

Breaking down the *no_pen* experiment into changes due to the orography and the land surface reveals the orography to be responsible for much of the circulation change. The Western Ghats are shown to be responsible for divergent flow as the Somali jet approaches from the south west, and considerable orographic rainfall. In addition, the Western Ghats add a considerable southerly component to the flow in the Bay of Bengal, just as the East African Highlands add a southerly component to flow in the Arabian Sea (Slingo *et al.*, 2005). Precipitation increases when orography is removed are particularly focused on the local maximum in the underlying SST forcing, over the southwest Bay of Bengal. Thus while the Himalayas aid the large-scale development of the monsoon via the mechanical separation of moist and dry sources of air (Boos and Kuang, 2010), the Western Ghats add important local detail to the circulation and regional distribution of precipitation.

Sensitivity tests made on the surface of the peninsula, with orography unperturbed, also reveal substantial impacts. Bare soil coverage does little to alter monsoon rainfall, there being a strong dry rainfall bias in the *control* anyway, while adding lake at the surface substantially increases monsoon rainfall by increasing the contribution of latent heat flux to the convergence of energy into the atmospheric column. Not only that, but both experiments with unlimited moisture (and high heat capacity) at the surface cause changes in the boundary layer evolution, smoothing out the diurnal cycle and increasing the prevalence of cumulus-capped boundary layers at the expense of stable and well-mixed types. Rainfall is increased at all times of day but particularly during the night. In addition to the local impacts on diurnal convection, we have also demonstrated that the surface conditions of the peninsula modulate the northward propagating modes of intraseasonal variability. This suggests that the mean state and variability are intrinsically linked (e.g. Sperber *et al.*, 2000).

By extending the region of perturbation north of the coastal boundary of the Indian Ocean, i.e., into the plains of the Indus and Ganges basins (IGP), we examine the role of roughly the whole South Asia region. Imposing a lake at the surface of the IGP region or over the whole of South Asia greatly enhances precipitation and the monsoon circulation. The increased rainfall is, in part, related to a greater number of monsoon depressions that are steered along the monsoon trough. This suggests a dual role for this region in terms of both moisture supply and local temperature and pressure gradients, which contribute to the structure and location of the monsoon trough. This is consistent with recent evidence that sources of moisture over northern India can be instrumental in extreme rainfall events, as in the case of the Pakistan floods of 2010 (Martius *et al.*, 2013).

When sea is prescribed over all of South Asia (*no_SA*), the role of the underlying SST distribution comes into play. The loss of the strong south-to-north temperature gradient as the IGP is approached limits the intensity of the monsoon trough and weakens the large-scale monsoon flow across the northern part of the Arabian Sea.

The effect of the peninsula on the strength and spatial and temporal distribution of the monsoon is substantial. The land and orography affect the flow through both surface roughness and low heat capacity, affecting seasonal and diurnal cycles of surface temperature as well as mean gradients of temperature, and therefore pressure. The temperature gradients south of the Himalayas appear to be crucial, a factor deserving further attention. Finally, moisture availability affects the depth, type and frequency of convection as well as playing a role in the evolution of surface temperature.

The study has demonstrated a useful diagnostic of boundary layer structure (defined according to the model formulation), which illustrates the tight locally and diurnally forced nature of the boundary layer structure in the current *control* model. However there is a pressing need for better characterisation of precipitation and the boundary layer, through better availability of high temporal and spatial resolution observed station data for the diurnal cycle of convection, and new observations with which to characterise the boundary layer evolution over India during the monsoon (see e.g. the use of Doppler lidar measurements in Harvey *et al.*, 2013). These would allow us to both better characterise the monsoon and validate our models or diagnose biases at these process scales.

Acknowledgements A. G. Turner is funded under a NERC Fellowship (NE/H015655/1) and also acknowledges NERC/MoES Changing Water Cycle projects SAPRISE (NE/I022469/1) and Hydroflux-India (NE/I022485/1). G. M. Martin and R. C. Levine were supported by the SAPRISE project and the Joint DECC/Defra Met Office Hadley Centre Climate Programme (GA01101). Computing resources for running MetUM GA3/GL3 were provided by HECToR.

References

Adler, R. F., Huffman, G. J., Chang, A., Ferraro, R., Xie, P. P., Janowiak, J., Rudolf, B., Schneider, U., Curtis, S., Bolvin, D., Gruber, A., Susskind, J., Arkin, P., and Nelkin, E. (2003). The version-2 global precipitation climatology project (GPCP) monthly precipitation analysis (1979-present). *Journal of Hydrometeorology*, **4**(6), 1147–1167.

Annamalai, H., Slingo, J. M., Sperber, K. R., and Hodges, K. (1999). The mean evolution and variability of the Asian summer monsoon: Comparison of ECMWF and NCEP-NCAR reanalyses. *Monthly Weather Review*, **127**(6), 1157–1186.

Best, M. J., Pryor, M., Clark, D. B., Rooney, G. G., Essery, R. L. H., Menard, C. B., Edwards, J. M., Hendry, M. A., Porson, A., Gedney, N., Mercado, L. M., Sitch, S., Blyth, E., Boucher, O., Cox, P. M., Grimmond, C. S. B., and Harding, R. J. (2011). The Joint UK Land Environment Simulator (JULES), model description - Part 1: Energy and water fluxes. *Geoscientific Model Development*, **4**(3), 677–699.

Bollasina, M. and Nigam, S. (2009). Indian Ocean SST, evaporation, and precipitation during the South Asian summer monsoon in IPCC-AR4 coupled simulations. *Climate Dynamics*, **33**(7-8).

Bollasina, M. and Nigam, S. (2011a). Modelling of regional hydroclimate change over the Indian subcontinent: Impact of the expanding Thar Desert. *Journal of Climate*, **24**(12), 3089–3106.

Bollasina, M. and Nigam, S. (2011b). The summertime ”heat” low over Pakistan/northwestern India: evolution and origin. *Climate Dynamics*, **37**(5-6), 957–970.

Boos, W. R. and Kuang, Z. (2010). Dominant control of the South Asian monsoon by orographic insulation versus plateau heating. *Nature*, **463**(7278), 218–U102.

Bowman, K. P., Collier, J. C., North, G. R., Wu, Q. Y., Ha, E. H., and Hardin, J. (2005). Diurnal cycle of tropical precipitation in Tropical Rainfall Measuring Mission (TRMM) satellite and ocean buoy rain gauge data. *Journal of Geophysical Research-Atmospheres*, **110**(D21).

Brown, A. R., Beare, R. J., Edwards, J. M., Lock, A. P., Keogh, S. J., Milton, S. F., and Walters, D. N. (2008). Upgrades to the boundary-layer scheme in the met office numerical weather prediction model. *Boundary-Layer Meteorology*, **128**(1), 117–132.

Bush, S. J., Turner, A. G., Martin, G., and Woolnough, S. J. (2013). The effect of increased entrainment on Asian monsoon biases in the MetUM General Circulation Model. *Quarterly Journal of the Royal Meteorological Society, submitted*.

Chou, C. and Neelin, J. D. (2003). Mechanisms limiting the northward extent of the northern summer monsoons over North America, Asia, and Africa. *Journal of Climate*, **16**(3), 406–425.

Chou, C., Neelin, J. D., and Su, H. (2001). Ocean-atmosphere-land feedbacks in an idealized monsoon. *Quarterly Journal of the Royal Meteorological Society*, **127**(576), 1869–1891.

Chung, C. E. and Ramanathan, V. (2006). Weakening of North Indian SST gradients and the monsoon rainfall in India and the Sahel. *Journal of Climate*, **19**(10), 2036–2045.

Clark, D. B., Mercado, L. M., Sitch, S., Jones, C. D., Gedney, N., Best, M. J., Pryor, M., Rooney, G. G., Essery, R. L. H., Blyth, E., Boucher, O., Harding, R. J., Huntingford, C., and Cox, P. M. (2011). The Joint UK Land Environment Simulator (JULES), model description - Part 2: Carbon fluxes and vegetation dynamics. *Geoscientific Model Development*, **4**(3), 701–722.

Dee, D. P., Uppala, S. M., Simmons, A. J., Berrisford, P., Poli, P., Kobayashi, S., Andrae, U., Balmaseda, M. A., Balsamo, G., Bauer, P., Bechtold, P., Beljaars, A. C. M., van de Berg, L., Bidlot, J., Bormann, N., Delsol, C., Dragani, R., Fuentes, M., Geer, A. J., Haimberger, L., Healy, S. B., Hersbach, H., Holm, E. V., Isaksen, L., Kallberg, P., Koehler, M., Matricardi, M., McNally, A. P., Monge-Sanz, B. M., Morcrette, J. J., Park, B. K., Peubey, C., de Rosnay, P., Tavolato, C., Thepaut, J. N., and Vitart, F. (2011). The ERA-Interim reanalysis: configuration and performance of the data assimilation system. *Quarterly Journal of the Royal Meteorological Society*, **137**(656), 553–597.

Duchon, C. E. (1979). Lanczos filtering in one and 2 dimensions. *Journal of Applied Meteorology*, **18**(8), 1016–1022.

Global Soil Data Task (2000). Global soil data products CD-ROM (IGBP-DIS). CD-ROM, International Geosphere-Biosphere Programme, Data and Information System, Potsdam, Germany. Available from Oak Ridge National Laboratory Distributed Active Archive Center, Oak Ridge, TN, available at: http://www.daac.ornl.gov.

Gregory, D. and Rowntree, P. R. (1990). A mass flux convection scheme with representation of cloud ensemble characteristics and stability-dependent closure. *Monthly Weather Review*, **118**(7), 1483–1506.

Harvey, N. J., Hogan, R. J., and Dacre, H. F. (2013). A method to diagnose boundary-layer type using Doppler lidar. *Quarterly Journal of the Royal Meteorogical Society*.

Hodges, K. I. (1994). A general method for tracking analysis and its application to meteorological data. *Monthly Weather Review*, **122**(11), 2573–2586.

Immerzeel, W. W., van Beek, L. P. H., and Bierkens, M. F. P. (2010). Climate Change Will Affect the Asian Water Towers. *Science*, **328**(5984), 1382–1385.

Ju, J. H. and Slingo, J. (1995). The Asian summer monsoon and ENSO. *Quarterly Journal of the Royal Meteorological Society*, **121**(525), 1133–1168.

Koster, R. D., Dirmeyer, P. A., Guo, Z. C., Bonan, G., Chan, E., Cox, P., Gordon, C. T., Kanae, S., Kowalczyk, E., Lawrence, D., Liu, P., Lu, C. H., Malyshev, S., McAvaney, B., Mitchell, K., Mocko, D., Oki, T., Oleson, K., Pitman, A., Sud, Y. C., Taylor, C. M., Verseghy, D., Vasic, R., Xue, Y. K., Yamada, T., and Team, G. (2004). Regions of strong coupling between soil moisture and precipitation. *Science*, **305**(5687), 1138–1140.

Krishnamurthy, V. and Ajayamohan, R. S. (2010). Composite Structure of Monsoon Low Pressure Systems and Its Relation to Indian Rainfall. *Journal of Climate*, **23**(16), 4285–4305.

Krishnamurthy, V. and Shukla, J. (2007). Intraseasonal and seasonally persisting patterns of Indian monsoon rainfall.

Journal of Climate, **20**(1), 3–20.

Levine, R. C. and Turner, A. G. (2012). Dependence of Indian monsoon rainfall on moisture fluxes across the Arabian Sea and the impact of coupled model sea surface temperature biases. *Climate Dynamics*, **38**(11-12), 2167–2190.

Levine, R. C., Turner, A. G., Marathayil, D., and Martin, G. M. (2013). The role of northern Arabian Sea surface temperature biases in CMIP5 model simulations and future projections of Indian summer monsoon rainfall. *Climate Dynamics*, **41**, 155–172.

Li, C. F. and Yanai, M. (1996). The onset and interannual variability of the Asian summer monsoon in relation to land sea thermal contrast. *Journal of Climate*, **9**(2), 358–375.

Lin, J.-L., Weickman, K. M., Kiladis, G. N., Mapes, B. E., Schubert, S. D., Suarez, M. J., Bacmeister, J. T., and Lee, M.-I. (2008). Subseasonal variability associated with Asian summer monsoon simulated by 14 IPCC AR4 coupled GCMs. *Journal of Climate*, **21**(18), 4541–4567.

Lock, A. P. (2001). The numerical representation of entrainment in parameterizations of boundary layer turbulent mixing. *Monthly Weather Review*, **129**(5), 1148–1163.

Lock, A. P., Brown, A. R., Bush, M. R., Martin, G. M., and Smith, R. N. B. (2000). A new boundary layer mixing scheme. Part I: Scheme description and single-column model tests. *Monthly Weather Review*, **128**(9), 3187–3199.

Marathayil, D., Turner, A. G., Shaffrey, L. C., and Levine, R. C. (2013). Systematic winter sea-surface temperature biases in the northern Arabian Sea in HiGEM and the CMIP3 models. *Environmental Research Letters*, **8**(1).

Martin, G. M. and Levine, R. C. (2012). The influence of dynamic vegetation on the present-day simulation and future projections of the South Asian summer monsoon in the HadGEM2 family. *Earth System Dynamics*, **3**, 245–261.

Martius, O., Sodemann, H., Joos, H., Pfahl, S., Winschall, A., Croci-Maspoli, M., Graf, M., Madonna, E., Mueller, B., Schemm, S., Sedlcek, J., Sprenger, M., and Wernli, H. (2013). The role of upper-level dynamics and surface processes for the Pakistan flood of July 2010. *Quarterly Journal of the Royal Meteorological Society*, pages 62–66.

Meehl, G. A., Covey, C., Delworth, T., Latif, M., McAvaney, B., Mitchell, J. F. B., Stouffer, R. J., and Taylor, K. E. (2007). The WCRP CMIP3 multimodel dataset - A new era in climate change research. *Bulletin of the American Meteorological Society*, **88**, 1383–+.

Molnar, P., England, P., and Martinod, J. (1993). Mantle dynamics, uplift of the Tibetan Plateau, and the Indian monsoon. *Reviews of Geophysics*, **31**(4), 357–396.

Niyogi, D., Kishtawal, C., Tripathi, S., and Govindaraju, R. S. (2010). Observational evidence that agricultural intensification and land use change may be reducing the Indian summer monsoon rainfall. *Water Resources Research*, **46**.

Prive, N. C. and Plumb, R. A. (2007). Monsoon dynamics with interactive forcing. Part I: Axisymmetric studies. *Journal of the Atmospheric Sciences*, **64**(5), 1417–1430.

Saeed, F., Hagemann, S., and Jacob, D. (2009). Impact of irrigation on the South Asian summer monsoon. *Geophysical Research Letters*, **36**.

Slingo, J., Spencer, H., Hoskins, B., Berrisford, P., and Black, E. (2005). The meteorology of the Western Indian Ocean, and the influence of the east African highlands. *Philosophical Transactions of the Royal Society a-Mathematical Physical and Engineering Sciences*, **363**(1826), 25–42.

Sperber, K. R., Slingo, J. M., and Annamalai, H. (2000). Predictability and the relationship between subseasonal and interannual variability during the Asian summer monsoon. *Quarterly Journal of the Royal Meteorological Society*, **126**(568), 2545–2574.

Sperber, K. R., Annamalai, H., Kang, I.-S., Kitoh, A., Moise, A., Turner, A., B., W., and Zhou, T. (2012). The Asian Summer Monsoon: An Intercomparison of CMIP5 vs. CMIP3 Simulations of the Late 20th Century. *Climate Dynamics*.

Taylor, K. E., Stouffer, R. J., and Meehl, G. A. (2012). An overview of CMIP5 and the experiment design. *Bulletin of the American Meteorological Society*, **93**(4), 485–498.

Tuinenburg, O. A., Hutjes, R. W. A., and Kabat, P. (2012). The fate of evaporated water from the Ganges basin. *Journal of Geophysical Research-Atmospheres*, **117**.

Turner, A. G. and Annamalai, H. (2012). Climate change and the South Asian summer monsoon. *Nature Climate Change*, **2**(8), 587–595.

Turner, A. G. and Slingo, J. M. (2009). Subseasonal extremes of precipitation and active-break cycles of the Indian summer monsoon in a climate-change scenario. *Quarterly Journal of the Royal Meteorological Society*, **135**(640), 549–567.

Turner, A. G., Joshi, M., Robertson, E. S., and Woolnough, S. J. (2012). The effect of Arabian Sea optical properties on SST biases and the South Asian summer monsoon in a coupled GCM. *Climate Dynamics*, **39**(3-4), 811–826.

Walters, D. N., Best, M. J., Bushell, A. C., Copsey, D., Edwards, J. M., Falloon, P. D., Harris, C. M., Lock, A. P., Manners, J. C., Morcrette, C. J., Roberts, M. J., Stratton, R. A., Webster, S., Wilkinson, J. M., Willett, M. R., Boutle, I. A., Earnshaw, P. D., Hill, P. G., MacLachlan, C., Martin, G. M., Moufouma-Okia, W., Palmer, M. D., Petch, J. C., Rooney, G. G., Scaife, A. A., and Williams, K. D. (2011). The Met Office Unified Model Global Atmosphere 3.0/3.1 and JULES Global Land 3.0/3.1 configurations. *Geoscientific Model Development*, **4**(4), 919–941.

Zhisheng, A., Kutzbach, J. E., Prell, W. L., and Porter, S. C. (2001). Evolution of Asian monsoons and phased uplift of the Himalaya-Tibetan plateau since Late Miocene times. *Nature*, **411**(6833), 62–66.